Modulation of Tropical Convection-circulation Interaction by Aerosol Indirect Effects in Idealized Simulations of a Global Convection-permitting Model

Chun-Yian Su[1], Chien-Ming Wu[2], Wei-Ting Chen[2], and John Peters[3]

[1]Pennsylvania State University
[2]National Taiwan University
[3]Penn State

October 17, 2023

Abstract

Observations suggest tropical convection intensifies when aerosol concentrations enhance, but quantitative estimations of this effect remain highly uncertain. Leading theories for explaining the influence of aerosol concentrations on tropical convection are based on the dynamical response of convection to changes in cloud microphysics, neglecting possible changes in the environment. In recent years, global convection-permitting models (GCPM) have been developed to circumvent problems arising from imposing artificial scale separation on physical processes associated with deep convection. Here, we use a GCPM to investigate how enhanced concentrations of aerosols that act as cloud condensate nuclei (CCN) impact tropical convection features by modulating the convection-circulation interaction. Results from a pair of idealized non-rotating radiative-convective equilibrium simulations show that the enhanced CCN concentration leads to weaker large-scale circulation, the closeness of deep convective systems to the moist cluster edges, and more mid-level cloud water at an equilibrium state in which convective self-aggregation occurred. Correspondingly, the enhanced CCN concentration modulates how the diabatic processes that support or oppose convective aggregation maintain the aggregated state at equilibrium. Overall, the enhanced CCN concentration facilitates the development of deep convection in a drier environment but reduces the large-scale instability and the convection intensity. Our results emphasize the importance of allowing atmospheric phenomena to evolve continuously across spatial and temporal scales in simulations when investigating the response of tropical convection to changes in cloud microphysics.

Modulation of Tropical Convection-circulation Interaction by Aerosol Indirect Effects in Idealized Simulations of a Global Convection-permitting Model

Chun-Yian Su[1,2], Chien-Ming Wu[2], Wei-Ting Chen[2], and John M. Peters[1]

[1]Department of Meteorology and Atmospheric Science, The Pennsylvania State University, University Park, PA
[2]Department of Atmospheric Sciences, National Taiwan University, Taipei city, Taiwan

Key Points:

- Tropical convection, large-scale circulation, and their responses to pollution are physical processes that couple together.
- Pollution leads to weaker large-scale circulation, the closeness of convection to the moist cluster edges, and more mid-level cloud water.
- Pollution facilitates deep convection development in a drier environment but reduces large-scale instability and convection intensity.

Corresponding author: Chun-Yian Su, `czs6237@psu.edu`

Abstract

Observations suggest tropical convection intensifies when aerosol concentrations enhance, but quantitative estimations of this effect remain highly uncertain. Leading theories for explaining the influence of aerosol concentrations on tropical convection are based on the dynamical response of convection to changes in cloud microphysics, neglecting possible changes in the environment. In recent years, global convection-permitting models (GCPM) have been developed to circumvent problems arising from imposing artificial scale separation on physical processes associated with deep convection. Here, we use a GCPM to investigate how enhanced concentrations of aerosols that act as cloud condensate nuclei (CCN) impact tropical convection features by modulating the convection-circulation interaction. Results from a pair of idealized non-rotating radiative-convective equilibrium simulations show that the enhanced CCN concentration leads to weaker large-scale circulation, the closeness of deep convective systems to the moist cluster edges, and more mid-level cloud water at an equilibrium state in which convective self-aggregation occurred. Correspondingly, the enhanced CCN concentration modulates how the diabatic processes that support or oppose convective aggregation maintain the aggregated state at equilibrium. Overall, the enhanced CCN concentration facilitates the development of deep convection in a drier environment but reduces the large-scale instability and the convection intensity. Our results emphasize the importance of allowing atmospheric phenomena to evolve continuously across spatial and temporal scales in simulations when investigating the response of tropical convection to changes in cloud microphysics.

Plain Language Summary

How does air pollution affect thunderstorm intensity over the tropical ocean? Past studies have proposed different opinions but generally neglect the interplay between the development of thunderstorms and the long-range movement of air that redistributes the Earth's thermal energy and moisture. Here, we address this question by investigating results from idealized numerical experiments in which the global domain is used to simultaneously simulate the response of individual thunderstorms and large-scale air motion to pollution. We found that pollution makes the thunderstorms keep less moisture in their surroundings, limiting the intensity of thunderstorms and weakening the large-scale air motion that supplies moisture to thunderstorms. Our results suggest that the interplay between the development of thunderstorms and the long-range movement of air is crucial in determining the effects of pollution in the tropical atmosphere.

1 Introduction

Tropical moist convection has long been recognized as a critical role in the global climate system (Arakawa, 2004; Hartmann et al., 2001). Various meteorological phenomena in the tropics are associated with the interaction between moist convection and atmospheric circulation, such as mesoscale convective systems (Houze, 2004) and convectively coupled waves (Kiladis et al., 2009; Lau & Lau, 1990). A deeper understanding of convection-circulation interaction across temporal and spatial scales is important for improving global climate predictions and forecasts of extreme precipitation events (Tomassini, 2020).

In recent years, several numerical modeling groups have developed global convection-permitting models (GCPMs) that explicitly simulate deep moist convection on the global domain to circumvent problems arising from parameterizations that presumably determine how circulations govern moist convection or how moist convection drives circulations (Caldwell et al., 2021; Hohenegger et al., 2023; Stevens et al., 2019). Interestingly, while the GCPMs capture basic aspects of the general circulation, they produce a diverse range of tropical convective systems (Feng et al., 2023; Su et al., 2022). For example, the distribution of tropical cloud modes varies greatly across the models (Nugent et al., 2022; Roh et al., 2021; Turbeville et al., 2022). The diversity in tropical convection features among the GCPMs has not been fully understood. One of the challenges to closing the knowledge gap is that the response of tropical convection and the large-scale circulation to any model treatment of subgrid-scale physical process (e.g., turbulence, microphysics) or natural and anthropogenic forcing are coupled throughout simulations. Hence, identifying the sensitivity of tropical convection-circulation to individual components or processes in the global climate system is critical to understanding the cause of the diverse tropical convection features among the GCPMs. Observations suggest that enhanced aerosol concentrations that arise from human activities and natural sources can substantially influence updrafts of tropical deep convection (Andreae et al., 2004; Koren et al., 2008; Niu & Li, 2012; Pan et al., 2021; Storer et al., 2014), but leading theories for explaining the influence neglects possible changes in the environment through convection-circulation interaction. In this study, we aim to investigate the impact of enhanced aerosol concentrations on tropical convection features using a GCPM.

By acting as cloud condensate nuclei (CCN) or ice nuclei (IN), aerosols change cloud properties by influencing cloud microphysics and dynamics, meanwhile influencing cloud-radiation feedbacks (i.e., aerosol indirect effects (AIEs); see reviews of Fan et al. (2016) and Tao et al. (2012)). However, the underlying mechanisms of how the updrafts are influenced remain elusive and are often debated (Fan et al., 2018; Fan & Khain, 2021; Grabowski & Morrison, 2020, 2021; Igel & van den Heever, 2021; J. M. Peters et al., 2023; Romps et al., 2023). A particular challenge of understanding AIEs using observations is that the observed aerosol concentrations in the environments of tropical deep convection often covary with other meteorological factors, such as convective available potential energy and vertical wind shear (Grabowski, 2018; Nishant & Sherwood, 2017; Varble, 2018), and the influences of meteorological and aerosol variability are difficult to disentangle from one another. Further, there is evidence from simulations that AIEs on deep convection vary as a function of meteorological conditions such as shear and humidity (Fan et al., 2009; van den Heever & Cotton, 2007; Khain et al., 2008; Koren et al., 2010; Lebo, 2018), which further complicates our ability to isolate the aerosol effects from other meteorological processes.

To take into account the interaction between tropical convection and the surrounding environment, Abbott and Cronin (2021) carried out simulations using a small domain (128x128 km^2) three-dimension cloud-resolving model (3-D CRM) with parameterized large-scale dynamics under the weak temperature gradient (WTG) approximation (Sobel et al., 2001). They suggested that enhanced aerosol concentrations produce clouds that mix more condensed water into the surrounding air. This enhances the environment favorably for subsequent convection by moistening the free troposphere and reducing the deleterious effects of entrainment. The humidity-entrainment mechanism they proposed is distinct from past work, which linked stronger updrafts with latent heat released by cloud condensation (Fan et al., 2018) or freezing (Rosenfeld et al., 2008) independently from possible changes in the environment. Using a similar modeling framework but under a different large-scale flow regime, Anber et al. (2019) found a contrasting result. In their simulations, convection and mean precipitation get weaker when the CCN concentration increases. They suggested that the changes are associated with the modulation of the coupling between convective processes and large-scale motions, which reduces surface enthalpy fluxes, rather than the changes in microphysical properties.

In CRM simulations that use a large domain for explicitly simulating the large-scale circulation between convecting and nonconvecting regions, results of AIEs on tropical convection have not reached a consensus as well. For example, van den Heever et al. (2011) found a weak response of the large-scale organization of convection and the domain-averaged precipitation to enhanced CCN concentrations in their 2-D CRM simulations (10000 km) configured in non-rotating radiative-convective equilibrium (RCE; Manabe & Strickler, 1964) with a fixed sea surface temperature (SST). They suggested that AIEs on the three tropical cloud modes are quite significant in magnitude and often opposite in sign, offsetting each other, thus producing a weak domain-wide response. In contrast, Beydoun and Hoose (2019) found a comparatively large decrease in domain-averaged precipitation with enhanced CCN concentrations in their RCE simulations of a channel-shaped (2000x120 km^2) 3-D CRM. They suggested that enhanced CCN concentrations weaken the large-scale organization of convection, leading to decreased domain-averaged precipitation. As discussed in Beydoun and Hoose (2019), the discrepancy between the results of the two studies may be caused by the difference in how the aerosol changes are imposed and the difference in model setup of domain geometry. Previous studies of RCE simulations found that the size of the simulation domain impacts the mechanisms that trigger and maintain the large-scale organization of convection (Jeevanjee & Romps, 2013; C. J. Muller & Held, 2012; Patrizio & Randall, 2019). A horizontal scale of model domain larger than 5000 km was suggested to be large enough to represent the natural scale of large-scale organization of convection and reach convergence of equilibrium states in simulations with different domain sizes (Matsugishi & Satoh, 2022; Yanase et al., 2022).

The goal of this study is to investigate how enhanced CCN concentration impacts tropical convection features through modulating the convection-circulation interaction using a GCPM that simultaneously simulates the dynamical response of tropical deep convection to changes in cloud microphysics and allows the large-scale organization of convection to naturally develop without artificial constraints due to domain size or shape. Idealized non-rotating RCE simulations with different scenarios of CCN concentration were carried out using the Central Weather Bureau Global Forecast System (CWBGFS; Su et al., 2021a).

Simulations configured in RCE have been extensively used to investigate feedbacks among clouds, environmental moisture, radiation, and precipitation (Bretherton et al., 2005; Coppin & Bony, 2015; Cronin & Wing, 2017; K. Emanuel et al., 2014; Holloway & Woolnough, 2016; Pendergrass et al., 2016; Popke et al., 2013; Singh & O'Gorman, 2013, 2015; Wing & Emanuel, 2014; Wing et al., 2020), providing an ideal experimental setting for our study. Previous studies found that convection in simulations configured in RCE can spontaneously self-organize into one or more moist ascending clusters surrounded by dry subsiding convection-free areas (convective self-aggregation (CSA); C. Muller et al., 2022; Wing et al., 2017). The occurrence of CSA changes the climate mean state dramatically (i.e., atmospheric heating and drying) and gives rise to the large-scale organization of convection that develops in line with the large-scale circulation. As will be shown later in this paper, CSA occurs in both of our simulations, but the degree of large-scale organization of convection changes with the enhancement of CCN concentration. We note that the terminologies of large-scale organization of convection and aggregation are used interchangeably in this paper, as they represent the same concept, at least in the scope of this study. The following section introduces more details about the model and our experiment design. Section 3 describes the results of the simulations when a statistical equilibrium is reached, and the summary and discussion are presented in section 4.

2 Model Description and Experiment Design

The Central Weather Bureau Global Forecast System (CWBGFS; Su et al., 2021a) is a global convection-permitting model that run at the horizontal resolution of around 15 km. Deep convection in the CWBGFS is represented by the unified relaxed Arakawa-Schubert scheme (URAS; Su et al., 2021b) in which the representation transitions from the parameterization to the explicit simulation as the diagnosed convective updraft fraction increases (Arakawa & Wu, 2013; Wu & Arakawa, 2014). Hence, the CWBGFS with the URAS can explicitly but efficiently simulate deep convection and the associated convection-circulation interaction on a global scale. The model partially resolves circulations in organized convective systems and reproduces the observed feature of convective systems that stronger extreme precipitation occurs in horizontally larger systems (Su et al., 2022).

In the CWBGFS, cloud microphysical processes, including cloud droplet activation, are represented by the two-moment Predicted Particle Properties bulk microphysics scheme (P3; Morrison & Milbrandt, 2015). Since the convective updraft fraction increases with updraft velocity so that the representation of deep convection transitions to explicit simulation as updraft enhances (Su et al., 2021b), we assume that taking cloud-aerosol interaction into account in the cloud model of URAS makes a small impact on the tropical convection features and will not change the conclusion of this study. On average, more than 93 % of precipitation is produced by explicitly simulated convection through the P3 scheme over precipitation events stronger than 5 mm h^{-1}. In the version of the P3 scheme used in this study, the aerosol is specified as a lognormal size distribution with a constant background aerosol concentration and mean size of 0.05 μm, consisting of ammonium sulfate. The number of activated CCN is a function of supersaturation given by Morrison and Grabowski (2007, 2008). The rest of the descriptions regarding physics suites and the dynamic core of the CWBGFS can be found in Su et al. (2021a).

We carried out two idealized non-rotating aqua-planet simulations configured in RCE with different constant background aerosol concentrations using the CWBGFS. Setting the background aerosol concentration as a constant provides us the simplest scenario for examining the changes in convection variability over space and the pattern of large-scale circulation with aerosol concentrations. As this study focuses on the AIEs, aerosols in the microphysics scheme do not interact with radiation. The current study sets the constant background aerosol concentration to 3x10^{8} kg^{-1} (pristine run) and 3x10^{10} kg^{-1} (polluted run) throughout the simulation, respectively. The scenarios here are referred to the marine environment (Andreae, 2009) and the urban environment (Chang et al., 2021). Previous studies suggested that tropical mean precipitation does not change with the enhancement of CCN concentration monotonically (van den Heever et al., 2011; Storer & van den Heever, 2013). Experiments with more diverse polluted scenarios will be carried out in the future.

The pristine run and the polluted run are initialized with the same analytic sounding (Wing et al., 2018) that approximates the moist tropical sounding of Dunion (2011), and the initial horizontal winds are set to zero. The initial surface pressure of all grid columns is 1014.8 hPa. The incoming solar radiation (409.6 W m^{-2}), the SST (300 K), and the surface albedo (0.07) are spatially uniform and remain constant in time. The simulations are run for 120 days, and the random perturbation of temperature from 0.1 to 0.02 K is added to the five lowest model levels in the first 20 days to speed up convection initiation. In the following section, we analyze results from day 100 to 120 when a statistical equilibrium state is met (Fig. S1) using hourly outputs. We note that the two runs may experience different transition processes to arrive at their equilibrium state, and a slow-phase oscillation of the global energy budget could exist. We assume that the probable presence of such a slow-phase oscillation would not change the conclusion of this study because the energy budget in both runs does not exhibit an obvious changing trend in the last 50 days of integration (Fig. S1).

3 Results

The RCE simulations in this study have typical features of CSA shown in the global model simulations of the RCE model intercomparison project (Wing et al., 2018, 2020), showing drying of the atmosphere and enhancement of spatial moisture variance. As convection self-organizing into multiple moist clusters, the global average of CWV decreases from the initial condition of 49.93 mm to the equilibrium state (day 100-120) of 29.96 mm in the pristine run and 29.73 mm in the polluted run (Fig. S1). Fig. 1 shows the spatial distribution of CWV at day 110. Both runs exhibit a high heterogeneity of CWV within moist clusters, which is coupled to convection. The pristine run has notably more occurrence of high CWV events (>60 mm). One can see that the CWV hotspots (>60 mm) in the pristine run occur over regions closer to the geometric center of each moist cluster than they do in the polluted run. We find that this particular feature may play an important role in the convection-circulation interaction, which will be investigated later in this paper.

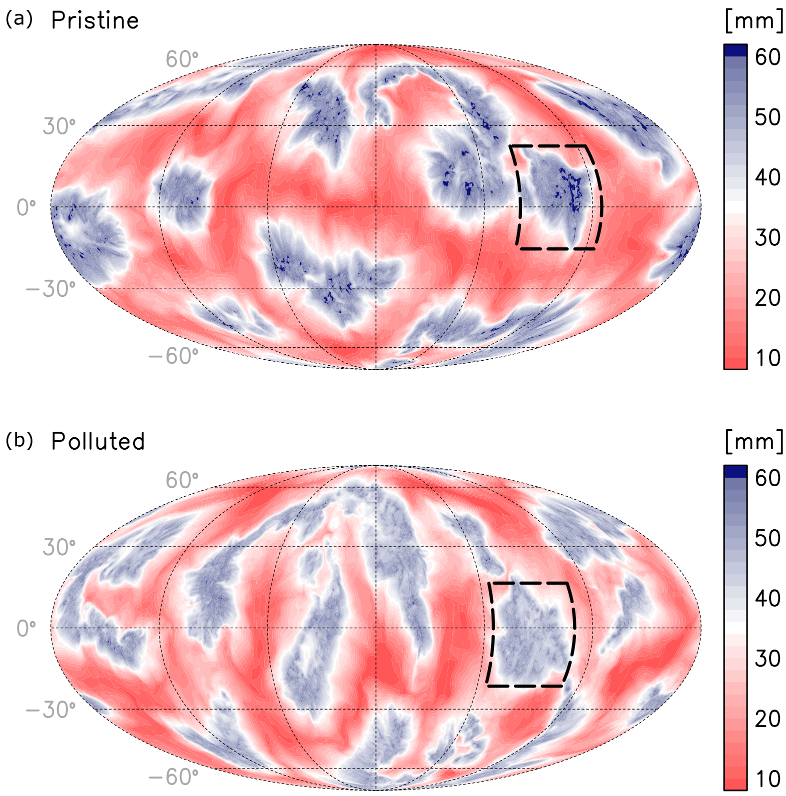

Figure 1. Spatial distribution of CWV at day 110 of the pristine run (a) and the polluted run (b).

At the equilibrium state, both runs exhibit a bimodal probability distribution of CWV (Fig. 2). The bimodality is associated with the presence of an aggregated state of convection (Tsai & Wu, 2017). The difference in CWV between the two local maxima of the bimodality is smaller in the polluted run, suggesting that the aggregated state in the polluted run is maintained by weaker large-scale circulation, and the aggregated state consists of drier moist clusters and wetter dry regions. Associated with the weakened large-scale circulation, the global averages of outward OLR and precipitation intensity at the equilibrium state are lower in the polluted run (287.45 W m^{-2}, 0.167 mm h^{-1}) than that in the pristine run (292.43 W m^{-2}, 0.174 mm h^{-1}). The polluted run has a colder temperature profile compared to that in the pristine run, with the largest difference of 1.7 K occurring at 200 hPa (Fig. S2). Meanwhile, the polluted run has the lower spatial variance of vertically integrated frozen moist static energy (FMSE) (1.03x10^{15} J^{2}m^{-4}) compared to that in the pristine run (1.32x10^{15} J^{2}m^{-4}). The FMSE has been used in studies of CSA to quantify the degree of aggregation

$$h = C_pT + gz + L_vq_v - L_fq_{ice}, \tag{1}$$

where C_p is the specific heat capacity of air, T is temperature, g is the gravitational acceleration, z is geopotential height, L_v is the latent heat of vaporization, q_v is the water vapor mixing ratio, L_f is the latent heat of fusion, and q_{ice} represents all ice phase condensates. During our analysis period, the variation in the spatial variance of vertically integrated FMSE with time in both runs is much less than the difference between the two runs (Fig. S3).

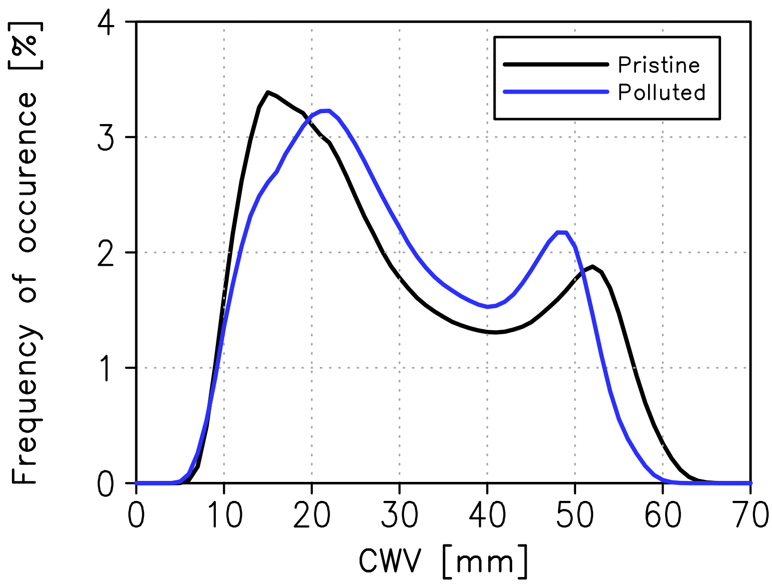

Figure 2. Probability distribution of CWV from days 100 to 120.

To identify the changes in energy transport between moist clusters and dry regions caused by pollution, we use the stream function on moisture space (Arnold & Putman, 2018)

$$\Psi_i(p) = \Psi_{i-1}(p) + \omega_i(p), \tag{2}$$

where p is pressure and ω_i is the pressure velocity averaged over the i^{th} CWV bin. Both runs in this study exhibit a shallow circulation, which transports moist static energy (MSE) upgradient, maintaining the large-scale organization of convection (Arnold & Putman, 2018; C. Muller et al., 2022), and a deep circulation, which exports MSE from moist ascending regions (Fig. 3a and 3b). While the deep circulation is directly driven by deep convection, the differential radiative cooling between moist clusters and dry regions (Fig. 3c and Fig. 3d) associated with the vertical gradients of relative humidity and clouds over dry regions (Fig. 3e and Fig. 3f) is believed to be one of the factors that drive shallow circulation in RCE simulations (C. J. Muller & Held, 2012). In general, the patterns of energy transport in the two runs are very much alike. The polluted run has the larger stream function at the upper free troposphere (300-400 hPa) compared to that in the pristine run (Fig. 3a and 3b), which suggests that the mean ascending motions are distributed wider in the moisture space when the environment is more polluted. However, the difference in the density of the stream function contours over there between the two runs is marginal. The difference in the low-level subsidence over dry regions between the two runs is also hard to be identified through Fig. 3a and 3b. We note that the polluted run has a higher cloud water mixing ratio over grid columns with CWV more than the 70$^{\text{th}}$ percentile compared to that in the pristine run, which is likely caused by enhanced cloud drop activation due to pollution.

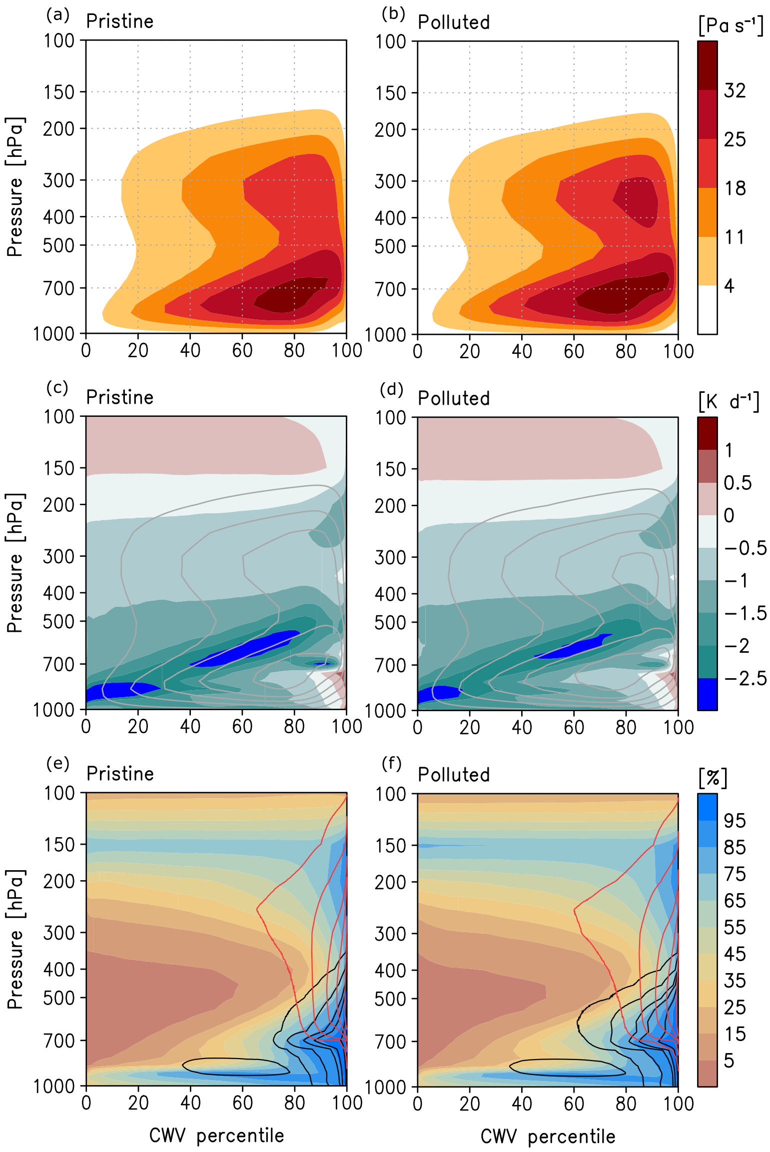

Figure 3. Vertical profiles of stream function (shaded) (a,b), radiative heating rate (shaded) (c,d), relative humidity (shaded), and cloud water (black) and cloud ice (red) mixing ratio contoured at 0.001, 0.01, 0.05, 0.1, 0.3 g kg^{-1} (e,f) conditionally sampled by CWV in the pristine run (left column) and the polluted run (right column) from day 100 to 120. The stream function in a,b is shown as contours in c,d.

As the stream function on moisture space does not represent physical horizontal flows, we further analyze the large-scale circulation on physical space in each run. We define moist clusters as contiguous grid columns with CWV >75$^{\text{th}}$ percentile in horizontal directions and dry regions as areas not defined as moist clusters. The 75$^{\text{th}}$ percentile of CWV is 42.34 mm in the pristine run and 40.75 mm in the polluted run. For each grid column, the distance to the edge of the nearest moist cluster with a spatial scale larger than 500 km (defined as the square root of horizontal area) is calculated. Horizontal winds at each vertical level are then projected to the direction pointing to the nearest edge and conditionally sampled by the distance to the edge. We neglect moist clusters smaller than 500 km because they are rare events that quickly dissipate or merge into larger moist clusters. The distance-binned projected horizontal wind speed and vertical velocity are shown in Fig. 4a and 4b. Negative distance values refer to areas inside the moist clusters as the distance is multiplied by -1 for grid columns belong a moist cluster.

The plot makes it clear that the polluted run has a weaker low-level inflow (below 850 hPa) from dry regions to moist clusters and a weaker high-level outflow (above 300 hPa) compared to those in the pristine run. Over moist clusters, the mean ascending motions are weaker and closer to the edge in the polluted run, but the difference in the maximum magnitude of the mean updrafts between the two runs is subtle. The mean CWV is homogeneous in regions within moist clusters but away from the edge ($d < -500\,km, d = distance\ to\ the\ nearest\ edge$) (Fig. 5a), while the distribution of the mean precipitation intensity is maximized near the edge (Fig. 5b) reflecting the distribution of the mean ascending motions. We speculate that the imprint of the changes in deep convection features caused by pollution on large-scale circulation is illustrated by analysis based on physical space rather than moisture space because the impact of pollution on deep convection intensity does not enhance or reduce monotonically to the increase in CWV.

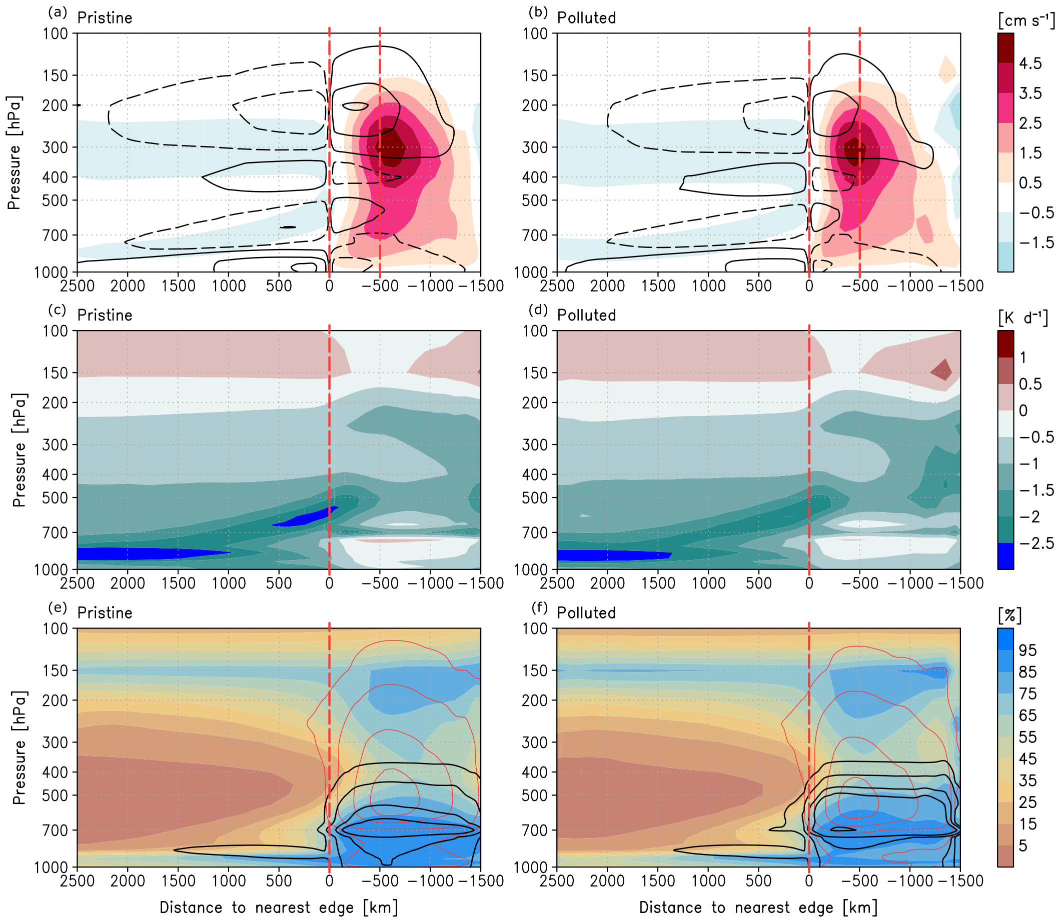

Figure 4. Vertical profiles of projected horizontal wind speed (contours at 0.5, 2.5, 4.5 m s^{-1}), vertical velocity (shaded) (a,b), radiative heating rate (shaded) (c,d), relative humidity (shaded), and cloud water (black) and cloud ice (red) mixing ratio contoured at 0.001, 0.01, 0.05, 0.1, 0.3 g kg^{-1} (e,f) conditionally sampled by the distance to the nearest edge in the pristine run (left column) and the polluted run (right column) from day 100 to 120. Projected horizontal wind pointing toward (away) the edge is shown by solid (dashed) contours. Negative distance values refer to areas inside the moist clusters

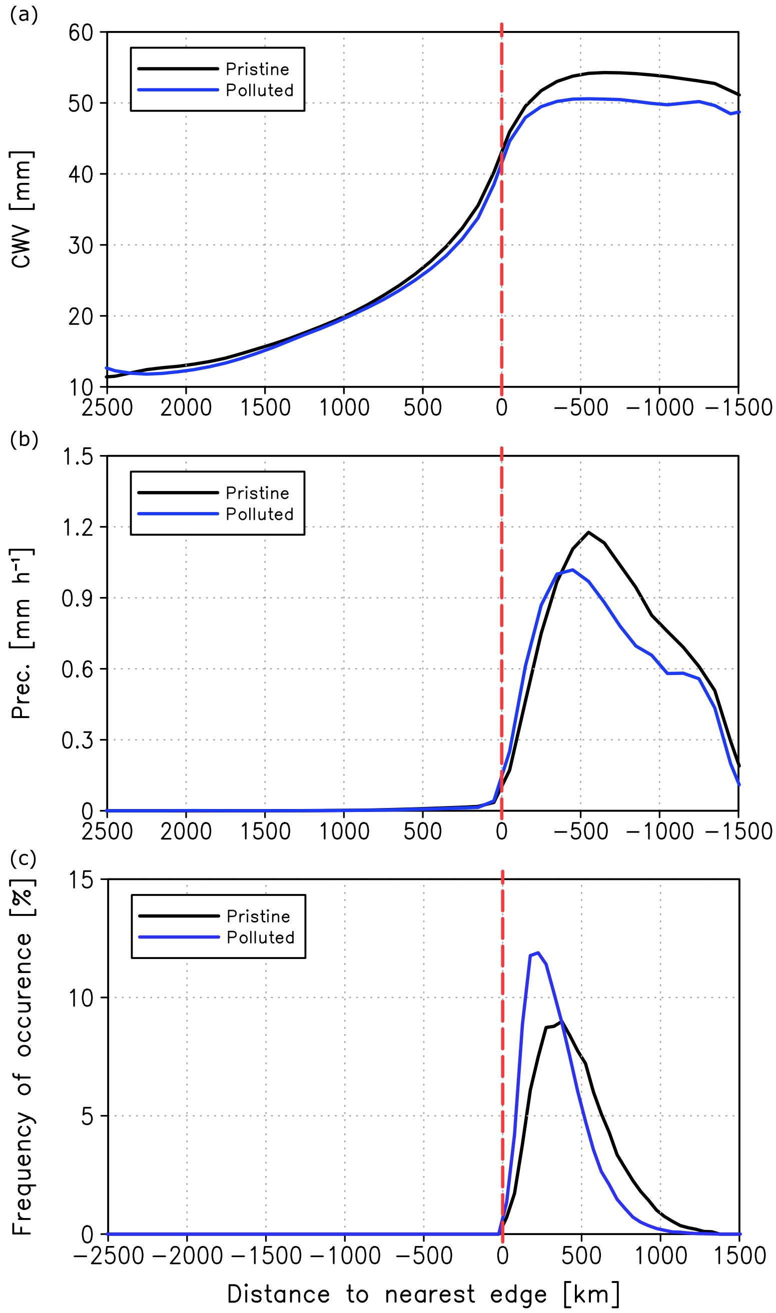

Figure 5. CWV (a), precipitation intensity (b), and the occurrence of explicitly simulated convection objects (c) conditionally sampled by the distance to the nearest edge from day 100 to 120.

We zoom in to one of the moist clusters to showcase the difference in the spatial distribution of convection between the two runs. Fig. 6a-d show the snapshots of vertical velocity at 500 hPa on top of CWV and precipitation intensity within the dashed rectangle shown in Fig. 1. In the polluted run, explicitly simulated convection develops over regions closer to the edge compared to that in the pristine run. This inference is further supported by the analysis of the distance from the geometric center of each convection object to its nearest edge (Fig. 5c), in which a convection object is defined as contiguous grid cells with vertical velocity at 500 hPa >0.1 m s^{-1}. In both runs, the highest probability of convection object occurrence is located at $-500 < d < 0\,km$.

Why are updrafts, especially those in the polluted run, preferably take place close to the edge? Intensification of tropical deep convection at the edge of convectively active regions has been identified by previous studies of observations (Mapes et al., 2018) and idealized RCE simulations (Becker et al., 2018; Windmiller & Hohenegger, 2019). Windmiller and Hohenegger (2019) proposed that the cause for the edge intensification is dynamical lifting by strong surface convergence that results from two opposing flows: a low-level inflow from dry regions to moist clusters and the propagation of continuously forming cold pools within moist clusters. Fig. 6e,f show the spatial distribution of the divergence field at 1000 hPa in our simulations. We can see the near-surface divergence collocates with updrafts, and strong near-surface convergence can be seen at regions between the edge and the existing updrafts. We speculate that the mechanism proposed by Windmiller and Hohenegger (2019) explains the edge intensification in our simulations, and the weaker low-level inflow in the polluted run may be one of the factors to polluted updrafts being closer to the edge. As will be shown later in this paper, pollution has a larger impact on the probability distribution of near-surface inflow than its impact on the probability distribution of the estimated cold pool propagation velocity in our simulations.

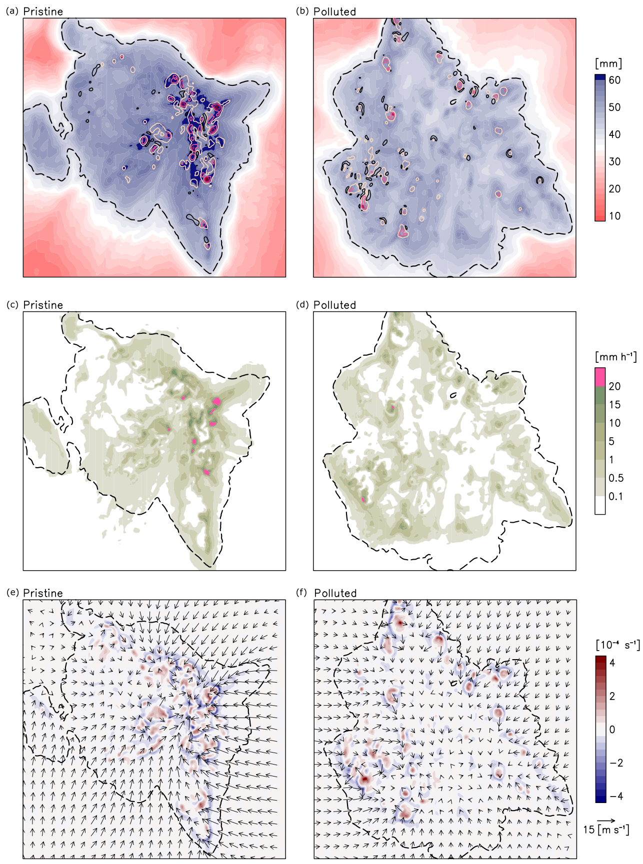

Figure 6. Spatial distribution of CWV, updraft velocity at 500 hPa (red scale, contoured at 0.1, 0.5, 1, 1.5 m s^{-1}), downdraft velocity at 500 hPa (black solid, contoured at 0.1 m s^{-1}) (a,b), precipitation intensity (c,d), and divergence field at 1000 hPa at day 110 of the pristine run (left column) and the polluted run (right column). The edge of the moist cluster (i.e., the 75$^{\text{th}}$ percentile of CWV) is demonstrated by black dashed lines.

Table 1. Spatial and temporal mean of each term in the right-hand side of eq.3

$[day^{-1}]$	Pristine moist clusters	Pristine dry regions	Polluted moist clusters	Polluted dry regions
Advection	-0.060	-0.007	-0.097	-0.004
SEF	-0.069	0.001	-0.045	-0.005
NetLW	0.065	-0.004	0.087	-0.001
NetSW	0.057	0.015	0.049	0.016

The distance-binned radiative heating rate, relative humidity, and hydrometeors mixing ratio over dry regions (Fig. 4c-f) resemble the CWV-binned results (Fig. 3c-f), except in physical space it is apparent that the polluted run has more mid-level (700 hPa) cloud water over the regions close to the edge ($0 < d < 500\,km$) than the pristine run does. The level of the cloud water coincides with the level of the outflow of shallow circulation from moist clusters, suggesting that polluted moist clusters export more cloud water to the dry regions than their pristine counterparts, and pollution may modulate the role of shallow circulation in maintaining the aggregated state.

To investigate the modulation of the diabatic processes that support or oppose convective aggregation by pollution, we analyze a budget of the spatial variance of FMSE at the equilibrium state as a quantitative account of the large-scale organization of convection following (Wing & Emanuel, 2014). The FMSE is a desirable diagnostic because vertically integrated FMSE can only be changed by radiation, surface fluxes, and advection. A process that contributes to the FMSE variance supports aggregation, and a process that reduces the FMSE variance opposes aggregation.

The budget equation of vertically integrated FMSE is given by eq. (9) in Wing and Emanuel (2014)

$$\frac{1}{2}\partial_t \hat{h}'^2 = -\hat{h}'\nabla_h \cdot \widehat{\overrightarrow{u}h} + \hat{h}'NetLW' + \hat{h}'NetSW' + \hat{h}'SEF', \tag{3}$$

where primes denote anomalies relative to the spatial mean and hats denote the mass-weighted column integral. $\hat{h}'$ is the anomaly of vertically integrated FMSE, $\nabla_h \cdot \widehat{\overrightarrow{u}h}$ represents the horizontal transport, $NetLW'$ is the anomaly of column longwave convergence, $NetSW'$ is the anomaly of column shortwave convergence, and SEF' is the anomaly of surface enthalpy fluxes. Each term in eq. (3) is calculated for each grid column using hourly outputs. We calculate the horizontal convergence term, the first term on the right-hand side, as a residual from the rest of the terms in eq. (3) following previous studies that have done FMSE budget calculations (Bretherton et al., 2005; C. J. Muller & Held, 2012; Wing & Emanuel, 2014). We arrive at an equation for the spatial variance by normalizing each term by the instantaneous horizontal mean of $\hat{h}'^2$. We then average each term over the analysis period (day 100-120) over moist clusters and dry regions, respectively. The result of the calculation is demonstrated in Table 1.

The diabatic processes over moist clusters are more dominant in maintaining the aggregated state than they do over dry regions, as Table 1 shows that the terms over moist clusters are much greater than those over dry regions in both runs. Hence, we focus on the diabatic processes over moist clusters in the following analysis. We can see that advection and surface enthalpy fluxes are the terms that oppose aggregation, while the radiation terms support aggregation. The negative value of the advection term indicates that the deep circulation, which represents a positive gross moist stability (Neelin & Held, 1987), governs the advection term so that the overall large-scale circulation tends to stabilize moist clusters. The polluted run has a greater negative value of the advection term compared to that in the pristine run. As the aforementioned results have demonstrated that the polluted run has weaker deep circulation, we suspect that the greater negative value of the advection term results from the reduction in the upgradient energy transport by shallow circulation. The primary factor of the reduction appears to be the greater export of cloud water at mid-level in the polluted run, as cloud water is implicitly taken into account by FMSE.

The negative value of surface enthalpy fluxes term in both runs suggests that the negative air-sea enthalpy disequilibrium feedback (Wing & Emanuel, 2014) overcomes the positive wind-induced surface heat exchange (WISHE; K. A. Emanuel, 1987) feedback in our model. Because our simulations use a fixed, uniform SST, the air-sea enthalpy disequilibrium depends on the near-surface water vapor mixing ratio. In the polluted run, the less column moisture over moist clusters may be responsible for the less negative value of the surface enthalpy fluxes term compared to the pristine run. As for the radiation terms, pollution leads to a greater value of the longwave term and a lower value of the shortwave term, of which more cloud cover emitting less energy outward and less column moisture absorbing less energy may be the primary factor, respectively. Overall, the budget analysis demonstrates that the modulation of how the diabatic processes that support or oppose convective aggregation maintain the aggregated state at equilibrium is consistent with the other results in this study. To further quantify the cause and effect of a certain process associated with AIEs, a different experiment setup with a focus on the transition between equilibrium states is necessary but out of the scope of this study.

The current result demonstrates that pollution modulates the relative role of shallow circulation in the overall energy transport under the equilibrium state with weaker large-scale circulation. The enhancement in the mid-level cloud water export from moist clusters appears to be a key factor of the modulation. The aforementioned result implies that the enhancement may be related to the closeness of the convection to the moist cluster edges.

The heterogeneity of convection over space in moist clusters illustrated in Fig. 1 and Fig. 6 suggests that isolating deep convection from the environment is necessary to elucidate the difference in bulk attributes of convection features between the polluted and the pristine run. We use the convective system identification method following Feng et al. (2019), defining cold cloud systems (CCSs) as contiguous grid cells with brightness temperature $T_b < 241\,K$. The OLR in our model outputs is converted to T_b following Yang and Slingo (2001). Fig.7 shows the mean vertical profiles of vertical velocity and hydrometeors mixing ratio within CCSs and the mean vertical profile of cloud water mixing ratio over regions in moist clusters but not defined as a CCS. We can see that the CCSs have top-heavy vertical profiles in both runs, while the polluted run has weaker mean vertical velocity (Fig. 7a). The weaker vertical velocities in the polluted run imply smaller condensation and deposition rates and lesser buoyancy production aloft. Consistent with this idea, there is less cloud ice within the polluted run (Fig. 7b). On the other hand, the enhanced CCN concentration results in a larger fraction of liquid occurring as cloud water (rather than rain). The polluted run has a cloud water mixing ratio more than twice that of the pristine run over both the CCSs and the other regions in moist clusters (Fig. 7c-d). The higher cloud water mixing ratio over regions outside of CCSs in the polluted run compared to that in the pristine run implies that pollution may lead to an increase in mid-level static stability, which promotes detrainment of cloud water into the environment (Johnson et al., 1999; Posselt et al., 2008).

The warm rain amount in the polluted run is less than that in the pristine run (Fig. 7e), which is an expected result (Rosenfeld, 1999). The polluted run has more falling rimed ice at the mid-to-low level (400-850 hPa) and the near-surface (Fig. 7f), showing that the partition between cold rain and warm rain may be different between the two runs. However, the impact of pollution on the mixed-phase microphysical processes can not be isolated from the other controlling factors in our simulations because the two runs have contrasting environmental conditions.

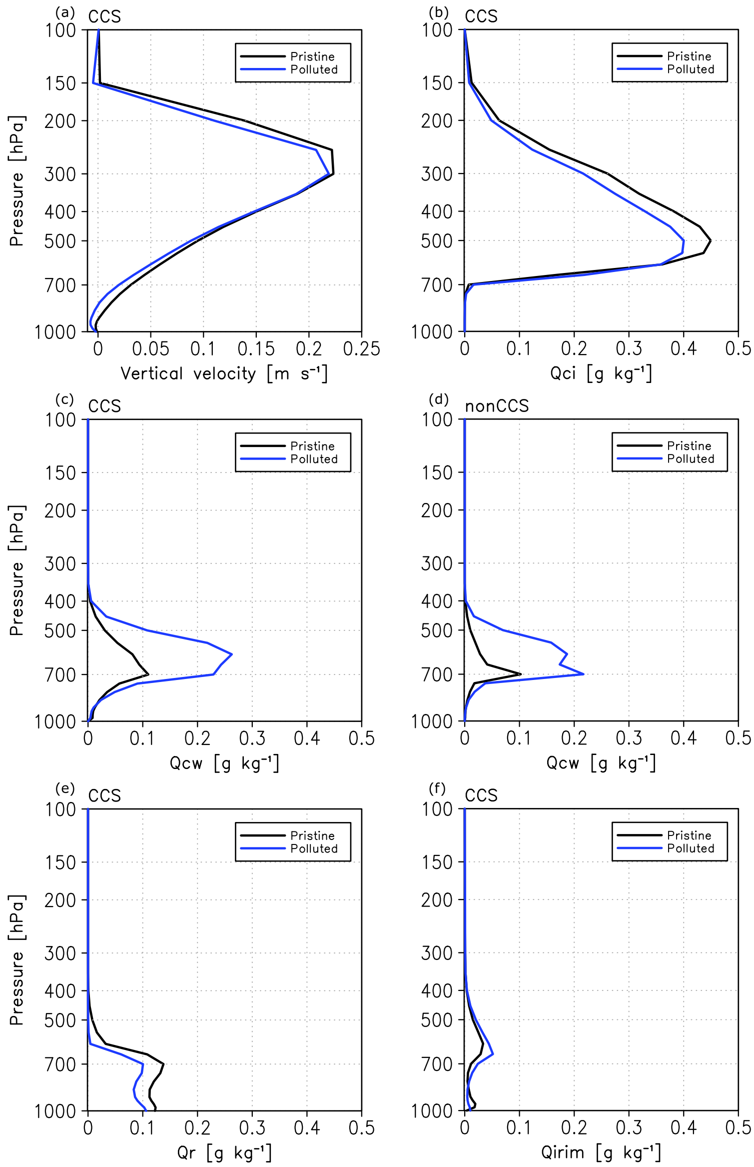

Figure 7. Vertical profiles of the mean vertical velocity and cloud ice, cloud water, rain water, and rimed cloud ice mixing ratio over the CCSs (a.b.c.e.f) and the mean profile of cloud water mixing ratio over the regions in moist clusters outside of CCSs (d).

A critical characteristic of tropical deep convection is the rapid intensification of precipitation once CWV has exceeded a critical value, which characterizes the effect of water vapor on the buoyancy of clouds through entrainment (Bretherton et al., 2004; Neelin et al., 2009; O. Peters & Neelin, 2006). We investigate the influence of pollution on this precipitation-CWV dependency. Analyses among all CCSs with a given CWV indicate that our simulations mimic the precipitation-CWV dependency seen in nature, with a rapid increase in precipitation (Fig. 8a) and updraft intensity (Fig. 8b-c) occurring above a certain threshold in CWV. However, a distinct difference between the polluted run and the pristine one is that the threshold CWV that heralds the increase in convective intensity occurs at a lower CWV value (53 mm) than it does in the pristine run (57 mm). On the other hand, the highest CWV environment over CCSs in the pristine run (>65 mm) is absent in the polluted run.

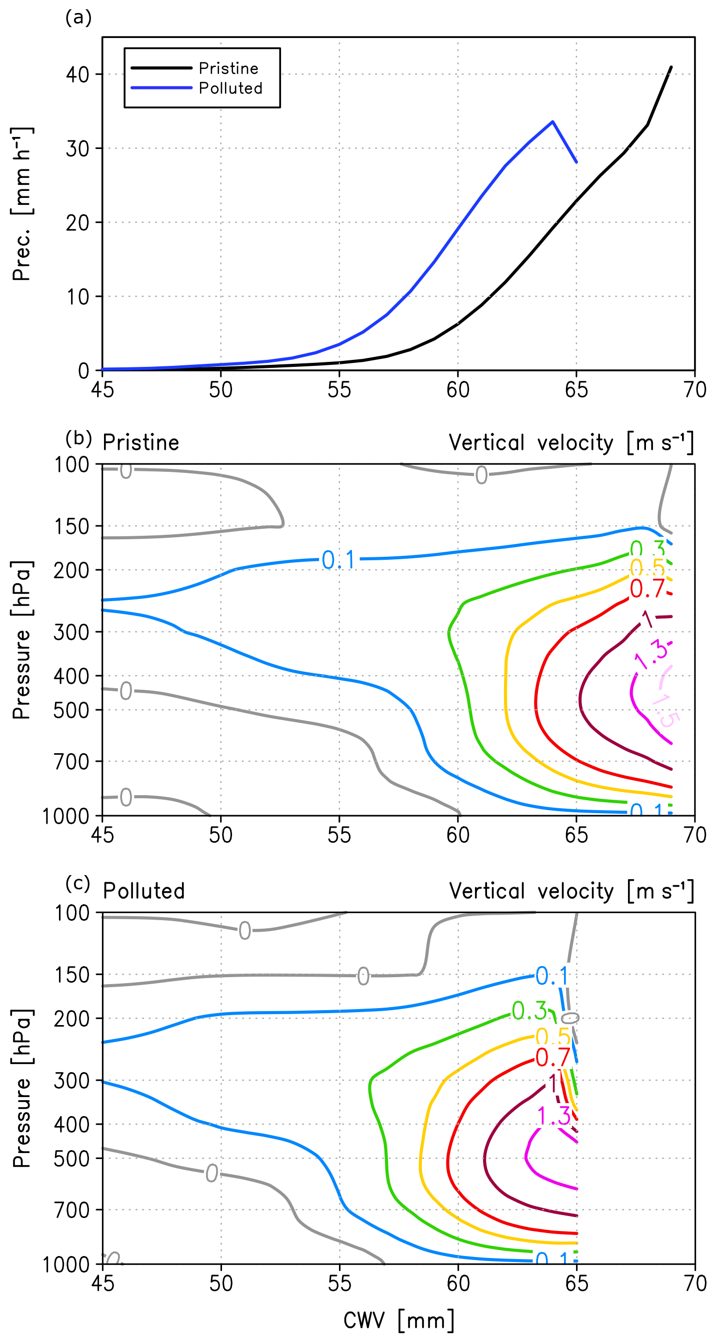

Figure 8. Precipitation intensity (a) and vertical velocity (b,c) within the CCSs conditional sampled by CWV from day 100 to 120.

Recall from Fig. 5a that mean CWV increases monotonically from dry regions toward moist clusters in both runs. We speculate that the spatial distribution of CCSs is a factor of the lower threshold CWV of rapid convection intensification in the polluted run. We apply the tracking analysis that links the CCSs overlapped in consecutive hourly outputs as a CCS track (Moseley et al., 2013) to find where CCSs start to develop. The tracked CCSs are classified into two categories according to how the CCS track initiates: emerging by itself and split from an existing CCS. Since our initiative is to identify the location where CCS triggering takes place, we only analyze the emerging tracks here.

Fig. 9 shows the distance-binned number of the emerging tracks with different present ages. The present age of a CCS is defined as the time difference between the present time step and the time step that the CCS emerged. In the polluted run, there are more tracks than the pristine run, and the maximum lifetime of the polluted tracks is longer. Tracks over dry regions have a shorter lifetime than tracks over moist clusters. The majority of young tracks (age<12 hr) in the polluted run are located at regions closer to the edge than they are in the pristine run. The result verifies our speculation that the CCSs in the polluted run start to develop at regions closer to the edge with a lower CWV at which strong near-surface convergence takes place.

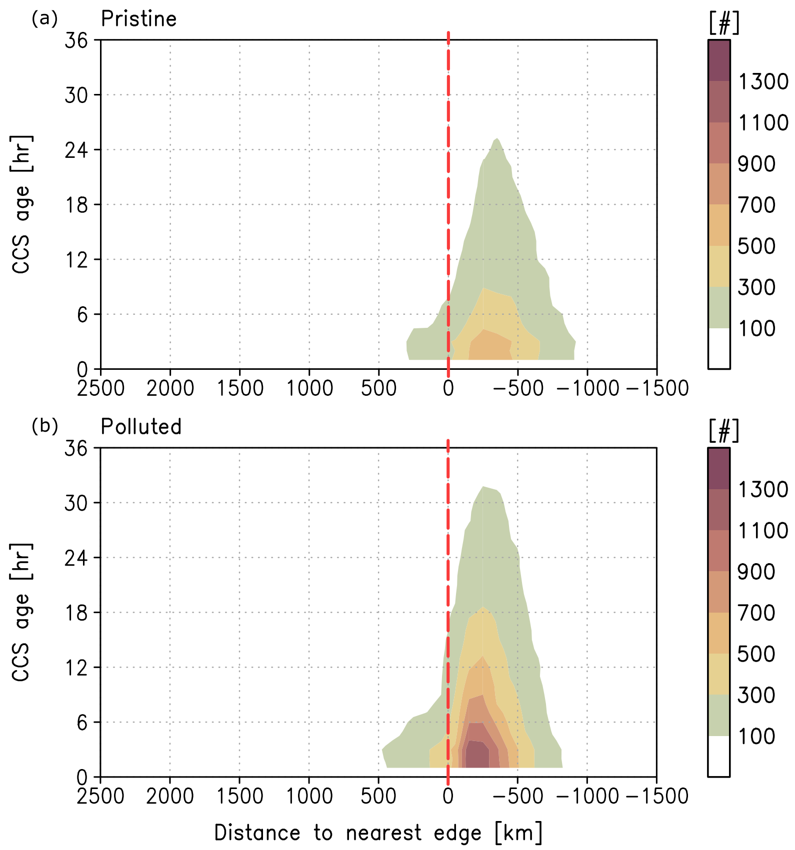

Figure 9. Number of CCSs with different present age (y-axis) conditionally sampled by the distance to the nearest edge in the pristine run (a) and the polluted run (b) from day 100 to 120.

Fig. 10a shows the probability distribution of the projected horizontal wind speed V_{in} at 1000 hPa over the regions of $0 < d < 50\,km$. Fig. 10b shows the probability distribution of the estimated cold pool propagation velocity (Rotunno et al., 1988) over the CCSs

$$V_{cp} = \sqrt{2\int_0^H -g\frac{\theta_\rho - \overline{\theta_\rho}(k)}{\overline{\theta_\rho}(k)}\,dz}, \tag{4}$$

where θ_ρ is the density potential temperature (K. A. Emanuel, 1994), k is the index of the moist cluster, overbars denote the average in k moist cluster but outside of CCSs, and H is the height of the cold pool given by the height at which θ_ρ is no longer smaller than $\overline{\theta_\rho}(k)$. As expected, the polluted run has the weaker V_{in} at 1000 hPa over the regions close to the edge. On the other hand, the impact of pollution on the distribution of estimated cold pool velocity is subtle. The distribution is slightly wider in the parameter space in the polluted run. We note that the analyses here are column-based, whereas V_{in} and V_{cp} were calculated using the mean fields over the regions close to the edge of moist clusters in Windmiller and Hohenegger (2019). The difference in how the analysis is performed may influence the resulting V_{in} and V_{cp} individually. Our result highlights that the weakening of near-surface inflow corroborates the closeness of the convection to the moist cluster edges in the polluted run, although the distribution of V_{in} does not approximately match the distribution of V_{cp} as shown in Fig. 8a in Windmiller and Hohenegger (2019).

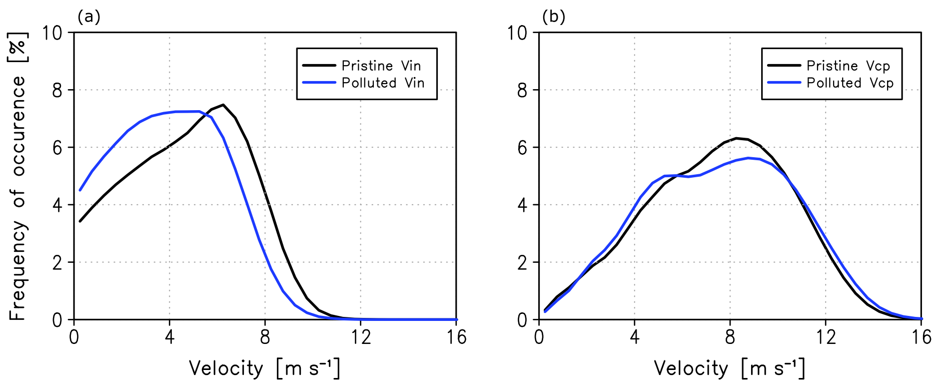

Figure 10. Probability distribution of V_{in} at 1000 hPa over the dry regions of $0 < d < 50\,km$ (a) and V_{cp} over the CCSs (b) from day 100 to 120.

Despite convection intensity starting to increase rapidly at a lower CWV in the polluted run, the two runs have the same increasing rate of convection intensity along with CWV. The CWV-binned precipitation intensities in the two runs can be collapsed by shifting the CWV by 4 mm. Why is the convection intensity limited in the polluted run (Fig. 7a)? We analyze the convective available potential energy (CAPE) for each moist cluster to identify the large-scale instability that constrains convection intensity. The CAPE is calculated as

$$CAPE_k = \int_{LFC}^{EL} B_k\,dz, \tag{5}$$

where k is the index of the moist cluster, LFC is the level of free convection, EL is the equilibrium level, and B_k is the buoyancy of the undiluted lifting parcel which is lifted adiabatically with freezing (J. M. Peters et al., 2022) from 2 m above ground level. The background environmental profile used for calculating B_k is the mean over regions within

k moist cluster but outside of CCSs. Fig. 11 shows the probability distribution of $CAPE$ of moist clusters larger than 500 km of horizontal scale. The result indicates that moist clusters in the polluted run generally have less large-scale instability. The suspected reduction in the upgradient energy transport by shallow circulation and the lower threshold CWV that may impede the accumulation of boundary layer moisture over moist clusters are both correlated to less CAPE in the polluted run. Overall, the polluted run has a weaker convection intensity compared to the pristine run.

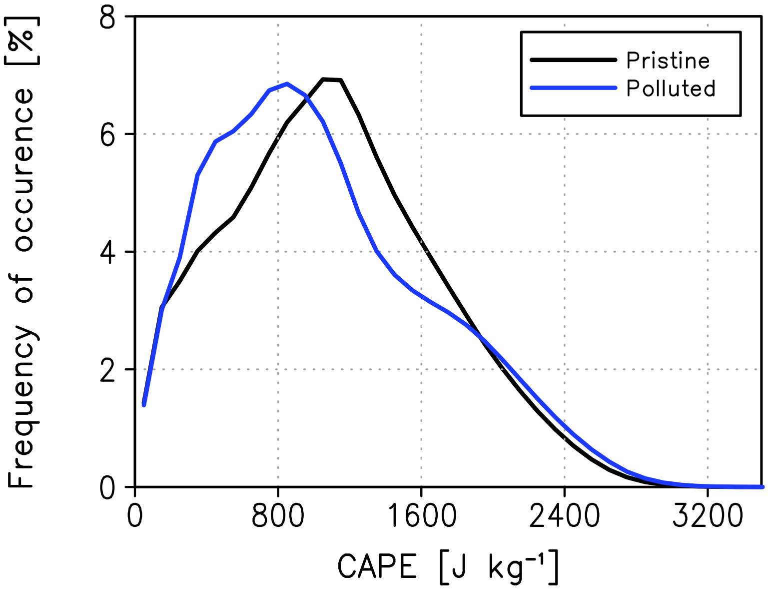

Figure 11. Moist cluster-based probability distribution of CAPE from day 100 to 120.

4 Summary and Discussion

This study investigates the modulation of tropical convection-circulation interaction by enhanced CCN concentrations using a pair of non-rotating RCE simulations with the uniform and fixed SST of 300K of a global convection-permitting model. The model explicitly simulates the dynamic response of deep convection to the enhanced CCN concentration and allows deep convection to interact with large-scale circulation without artificial constraints of scale separation assumption and the geometry of the simulation domain. The idealized setup of constant background aerosol concentration in the two simulations, namely the pristine run and the polluted run, is used to examine the changes in convection variability over space and the pattern of large-scale circulation with pollution. We analyze the difference between the pristine run and the polluted run at a statistical equilibrium state of RCE in which the convective self-aggregation processes had occurred, resulting in an aggregated state maintained by large-scale circulations.

We found that pollution weakens large-scale circulations, including the deep circulation and the shallow circulation, and leads to a mean state with a lower degree of convective aggregation. Analysis of cold cloud systems tracking shows that deep convective systems in the polluted run have notably more mid-level cloud water compared to the pristine run, and they preferably start to develop over regions close to the edge of moist clusters, contributing to the export of cloud water from moist clusters to dry regions. Pollution modulates how the diabatic processes that support or oppose convective aggregation maintain the aggregated state at equilibrium, including the role of shallow circulation in the energy transport between moist clusters and dry regions. Overall, the analysis of precipitation-CWV dependency suggests that pollution facilitates the development of deep convection in a drier environment but reduces the large-scale instability and the convection intensity. Our results emphasize the importance of allowing atmospheric phenomena to evolve continuously across spatial and temporal scales in simulations when investigating the response of tropical convection to changes in cloud microphysics. To our knowledge, this is the first study that simultaneously simulates the response of deep convection to changes in cloud microphysics and postulates the impact of pollution on the interaction between system-based tropical convection features and large-scale circulation that develops without the limitation of horizontal scale.

Similarities between our results and previous studies of aerosol indirect effects on tropical troposphere include weakened convection intensity (Beydoun & Hoose, 2019; Morrison & Grabowski, 2011), atmospheric cooling (Nishant et al., 2019; Dagan, 2022), and weakened convective aggregation (Beydoun & Hoose, 2019). However, there are contrasting physical processes leading to the results. For example, enhanced high clouds amount due to pollution leading to weaker tropospheric destabilization through radiative effects are found critical to weakening convection in Morrison and Grabowski (2011) and Beydoun and Hoose (2019). The polluted run has a less high cloud amount compared to the pristine run in this study (Fig. 4 and Fig. 7). We suspect that the contrasting result in the dependence of high clouds amount to pollution may be model dependent since the representation of mixed-phase microphysical processes is believed to drive the large difference in tropical high clouds among the GCPMs (Nugent et al., 2022; Roh et al., 2021; Turbeville et al., 2022). The equilibrium state analysis here provides a reference for studies aiming at finding causal relationships between physical processes. An investigation focusing on the transition phase between different aggregated states due to pollution will be carried out by the co-authors.

The current model runs at the horizontal resolution of around 15 km so that the minimum scale of deep convection development is close to the scale of convective updraft cores within an organized convective system (Houze, 2018). While we focus on the changes in the multi-scale coupling processes associated with the response of tropical deep convection to pollution, the study of van den Heever et al. (2011) suggested that aerosol indirect effects associated with tropical shallow clouds may offset or compensate for the aerosol indirect effects associated with congestus and deep convection systems and vice versa. We expect studies with the inclusion of the response of shallow convection to pollution using the current research framework to come in the future. Parallel modeling efforts to further depict the natural variability include heterogeneous aerosol perturbations, cloud-aerosol interactions, air-sea interactions, and aerosol direct radiative effects.

A possible real-world manifestation of our result is the convection activity over the Maritime Continent (MC) region. Past studies indicated that the large-scale organization of convection in non-rotating RCE simulations and MJO-like (i.e., Madden-Julian Oscillation; Madden & Julian, 1971) disturbance in rotating RCE simulations share the same driving mechanism (i.e., cloud-radiation feedbacks) in which AIEs can be critical (Arnold & Randall, 2015; Khairoutdinov & Emanuel, 2018). One of the leading theories of MJO propagation is that MJOs suffer from a barrier effect when they propagate over the MC (Kim et al., 2014; Zhang & Ling, 2017). The development of convective systems over the ocean in the MC plays a crucial role in carrying the MJO signal (Ling et al., 2019). As the MC is a major source of different types of aerosol around the globe (Reid et al., 2012; Salinas et al., 2013; Shpund et al., 2019), evaluation of sub-seasonal hindcasts spanning an active MJO event can be carried out to investigate the observed relationship between the geographical distribution of convective systems and aerosol emission scenarios.

5 Open Research

A temporal snapshot of CWV, grid column distance to the nearest moist cluster edge, CCS, and the GrADS plotting scripts are available at https://doi.org/10.6084/m9.figshare.22149617.v2.

Acknowledgments

Chun-Yian Su and J. Peter's efforts were supported by National Science Foundation (NSF) grants AGS-1928666, AGS-1841674, and the Department of Energy Atmospheric System Research (DOE ASR) grant DE-SC0000246356. Chien-Ming Wu and Chun-Yian Su's efforts were supported by National Science and Technology Council of Taiwan grant 111-2111-M-002-012-NSTC. Wei-Ting Chen was supported by National Science and Technology Council of Taiwan grants NSTC112-2111-M-002-008, NSTC112-2111-M-002-015, and National Taiwan University grants NTU-112L7832 and NTU-112L7858. We thank Dr. Jen-Her Chen in Central Weather Bureau for his support of this work.

References

Abbott, T. H., & Cronin, T. W. (2021, January). Aerosol invigoration of atmospheric convection through increases in humidity. *Science*, *371*(6524), 83–85. Retrieved from `https://doi.org/10.1126/science.abc5181` doi: 10.1126/science.abc5181

Anber, U. M., Wang, S., Gentine, P., & Jensen, M. P. (2019, September). Probing the response of tropical deep convection to aerosol perturbations using idealized cloud-resolving simulations with parameterized large-scale dynamics. *Journal of the Atmospheric Sciences*, *76*(9), 2885–2897. Retrieved from `https://doi.org/10.1175/jas-d-18-0351.1` doi: 10.1175/jas-d-18-0351.1

Andreae, M. O. (2009, January). Correlation between cloud condensation nuclei concentration and aerosol optical thickness in remote and polluted regions. *Atmospheric Chemistry and Physics*, *9*(2), 543–556. Retrieved from `https://doi.org/10.5194/acp-9-543-2009` doi: 10.5194/acp-9-543-2009

Andreae, M. O., Rosenfeld, D., Artaxo, P., Costa, A. A., Frank, G. P., Longo, K. M., & Silva-Dias, M. A. F. (2004, February). Smoking rain clouds over the amazon. *Science*, *303*(5662), 1337–1342. Retrieved from `https://doi.org/10.1126/science.1092779` doi: 10.1126/science.1092779

Arakawa, A. (2004, July). The cumulus parameterization problem: Past, present, and future. *Journal of Climate*, *17*(13), 2493–2525. Retrieved from `https://doi.org/10.1175/1520-0442(2004)017<2493:ratcpp>2.0.co;2` doi: 10.1175/1520-0442(2004)017⟨2493:ratcpp⟩2.0.co;2

Arakawa, A., & Wu, C.-M. (2013, July). A unified representation of deep moist convection in numerical modeling of the atmosphere. part i. *Journal of the Atmospheric Sciences*, *70*(7), 1977–1992. Retrieved from `https://doi.org/10.1175/jas-d-12-0330.1` doi: 10.1175/jas-d-12-0330.1

Arnold, N. P., & Putman, W. M. (2018, April). Nonrotating convective self-aggregation in a limited area AGCM. *Journal of Advances in Modeling Earth Systems*, *10*(4), 1029–1046. Retrieved from `https://doi.org/10.1002/2017ms001218` doi: 10.1002/2017ms001218

Arnold, N. P., & Randall, D. A. (2015, October). Global-scale convective aggregation: Implications for the madden-julian oscillation. *Journal of Advances in Modeling Earth Systems*, *7*(4), 1499–1518. Retrieved from `https://doi.org/10.1002/2015ms000498` doi: 10.1002/2015ms000498

Becker, T., Bretherton, C. S., Hohenegger, C., & Stevens, B. (2018, January). Estimating bulk entrainment with unaggregated and aggregated convection. *Geophysical Research Letters*, *45*(1), 455–462. Retrieved from `https://doi.org/10.1002/2017gl076640` doi: 10.1002/2017gl076640

Beydoun, H., & Hoose, C. (2019, April). Aerosol-cloud-precipitation interactions in the context of convective self-aggregation. *Journal of Advances in Modeling Earth Systems*, *11*(4), 1066–1087. Retrieved from https://doi.org/10.1029/2018ms001523 doi: 10.1029/2018ms001523

Bretherton, C. S., Blossey, P. N., & Khairoutdinov, M. (2005, December). An energy-balance analysis of deep convective self-aggregation above uniform SST. *Journal of the Atmospheric Sciences*, *62*(12), 4273–4292. Retrieved from https://doi.org/10.1175/jas3614.1 doi: 10.1175/jas3614.1

Bretherton, C. S., Peters, M. E., & Back, L. E. (2004, April). Relationships between water vapor path and precipitation over the tropical oceans. *Journal of Climate*, *17*(7), 1517–1528. Retrieved from https://doi.org/10.1175/1520-0442(2004)017<1517:rbwvpa>2.0.co;2 doi: 10.1175/1520-0442(2004)017⟨1517:rbwvpa⟩2.0.co;2

Caldwell, P. M., Terai, C. R., Hillman, B., Keen, N. D., Bogenschutz, P., Lin, W., … Zender, C. S. (2021, November). Convection-permitting simulations with the e3sm global atmosphere model. *Journal of Advances in Modeling Earth Systems*, *13*(11). Retrieved from https://doi.org/10.1029/2021ms002544 doi: 10.1029/2021ms002544

Chang, Y.-H., Chen, W.-T., Wu, C.-M., Moseley, C., & Wu, C.-C. (2021, November). Tracking the influence of cloud condensation nuclei on summer diurnal precipitating systems over complex topography in taiwan. *Atmospheric Chemistry and Physics*, *21*(22), 16709–16725. Retrieved from https://doi.org/10.5194/acp-21-16709-2021 doi: 10.5194/acp-21-16709-2021

Coppin, D., & Bony, S. (2015, December). Physical mechanisms controlling the initiation of convective self-aggregation in a general circulation model. *Journal of Advances in Modeling Earth Systems*, *7*(4), 2060–2078. Retrieved from https://doi.org/10.1002/2015ms000571 doi: 10.1002/2015ms000571

Cronin, T. W., & Wing, A. A. (2017, December). Clouds, circulation, and climate sensitivity in a radiative-convective equilibrium channel model. *Journal of Advances in Modeling Earth Systems*, *9*(8), 2883–2905. Retrieved from https://doi.org/10.1002/2017ms001111 doi: 10.1002/2017ms001111

Dagan, G. (2022, December). Equilibrium climate sensitivity increases with aerosol concentration due to changes in precipitation efficiency. *Atmospheric Chemistry and Physics*, *22*(24), 15767–15775. Retrieved from https://doi.org/10.5194/acp-22-15767-2022 doi: 10.5194/acp-22-15767-2022

Dunion, J. P. (2011, February). Rewriting the climatology of the tropical north atlantic and caribbean sea atmosphere. *Journal of Climate*, *24*(3), 893–908. Retrieved from https://doi.org/10.1175/2010jcli3496.1 doi: 10.1175/2010jcli3496.1

Emanuel, K., Wing, A. A., & Vincent, E. M. (2014, February). Radiative-convective instability. *Journal of Advances in Modeling Earth Systems*, *6*(1), 75–90. Retrieved from https://doi.org/10.1002/2013ms000270 doi: 10.1002/2013ms000270

Emanuel, K. A. (1987, August). An air-sea interaction model of intraseasonal oscillations in the tropics. *Journal of the Atmospheric Sciences*, *44*(16), 2324–2340. Retrieved from https://doi.org/10.1175/1520-0469(1987)044<2324:aasimo>2.0.co;2 doi: 10.1175/1520-0469(1987)044⟨2324:aasimo⟩2.0.co;2

Emanuel, K. A. (1994). *Atmospheric convection*. Oxford University Press, USA.

Fan, J., & Khain, A. (2021, January). Comments on "do ultrafine cloud condensation nuclei invigorate deep convection?". *Journal of the Atmospheric Sciences*, *78*(1), 329–339. Retrieved from https://doi.org/10.1175/jas-d-20-0218.1 doi: 10.1175/jas-d-20-0218.1

Fan, J., Rosenfeld, D., Zhang, Y., Giangrande, S. E., Li, Z., Machado, L. A. T., … de Souza, R. A. F. (2018, January). Substantial convection and precipitation enhancements by ultrafineaerosol particles. *Science*, *359*(6374), 411–418. Retrieved from https://doi.org/10.1126/science.aan8461 doi:

10.1126/science.aan8461
Fan, J., Wang, Y., Rosenfeld, D., & Liu, X. (2016, October). Review of aerosol–cloud interactions: Mechanisms, significance, and challenges. *Journal of the Atmospheric Sciences*, *73*(11), 4221–4252. Retrieved from `https://doi.org/10.1175/jas-d-16-0037.1` doi: 10.1175/jas-d-16-0037.1
Fan, J., Yuan, T., Comstock, J. M., Ghan, S., Khain, A., Leung, L. R., … Ovchinnikov, M. (2009, November). Dominant role by vertical wind shear in regulating aerosol effects on deep convective clouds. *Journal of Geophysical Research*, *114*(D22). Retrieved from `https://doi.org/10.1029/2009jd012352` doi: 10.1029/2009jd012352
Feng, Z., Houze, R. A., Leung, L. R., Song, F., Hardin, J. C., Wang, J., … Homeyer, C. R. (2019, September). Spatiotemporal characteristics and large-scale environments of mesoscale convective systems east of the rocky mountains. *Journal of Climate*, *32*(21), 7303–7328. Retrieved from `https://doi.org/10.1175/jcli-d-19-0137.1` doi: 10.1175/jcli-d-19-0137.1
Feng, Z., Leung, L. R., Hardin, J., Terai, C. R., Song, F., & Caldwell, P. (2023, February). Mesoscale convective systems in DYAMOND global convection-permitting simulations. *Geophysical Research Letters*, *50*(4). Retrieved from `https://doi.org/10.1029/2022gl102603` doi: 10.1029/2022gl102603
Grabowski, W. W. (2018, October). Can the impact of aerosols on deep convection be isolated from meteorological effects in atmospheric observations? *Journal of the Atmospheric Sciences*, *75*(10), 3347–3363. Retrieved from `https://doi.org/10.1175/jas-d-18-0105.1` doi: 10.1175/jas-d-18-0105.1
Grabowski, W. W., & Morrison, H. (2020, July). Do ultrafine cloud condensation nuclei invigorate deep convection? *Journal of the Atmospheric Sciences*, *77*(7), 2567–2583. Retrieved from `https://doi.org/10.1175/jas-d-20-0012.1` doi: 10.1175/jas-d-20-0012.1
Grabowski, W. W., & Morrison, H. (2021, January). Reply to "comments on 'do ultrafine cloud condensation nuclei invigorate deep convection?'". *Journal of the Atmospheric Sciences*, *78*(1), 341–350. Retrieved from `https://doi.org/10.1175/jas-d-20-0315.1` doi: 10.1175/jas-d-20-0315.1
Hartmann, D. L., Moy, L. A., & Fu, Q. (2001, December). Tropical convection and the energy balance at the top of the atmosphere. *Journal of Climate*, *14*(24), 4495–4511. Retrieved from `https://doi.org/10.1175/1520-0442(2001)014<4495:tcateb>2.0.co;2` doi: 10.1175/1520-0442(2001)014⟨4495:tcateb⟩2.0.co;2
Hohenegger, C., Korn, P., Linardakis, L., Redler, R., Schnur, R., Adamidis, P., … Stevens, B. (2023, January). ICON-sapphire: simulating the components of the earth system and their interactions at kilometer and subkilometer scales. *Geoscientific Model Development*, *16*(2), 779–811. Retrieved from `https://doi.org/10.5194/gmd-16-779-2023` doi: 10.5194/gmd-16-779-2023
Holloway, C. E., & Woolnough, S. J. (2016, February). The sensitivity of convective aggregation to diabatic processes in idealized radiative-convective equilibrium simulations. *Journal of Advances in Modeling Earth Systems*, *8*(1), 166–195. Retrieved from `https://doi.org/10.1002/2015ms000511` doi: 10.1002/2015ms000511
Houze, R. A. (2004, December). Mesoscale convective systems. *Reviews of Geophysics*, *42*(4). Retrieved from `https://doi.org/10.1029/2004rg000150` doi: 10.1029/2004rg000150
Houze, R. A. (2018, January). 100 years of research on mesoscale convective systems. *Meteorological Monographs*, *59*, 17.1–17.54. Retrieved from `https://doi.org/10.1175/amsmonographs-d-18-0001.1` doi: 10.1175/amsmonographs-d-18-0001.1
Igel, A. L., & van den Heever, S. C. (2021, August). Invigoration or enervation of convective clouds by aerosols? *Geophysical Research Letters*, *48*(16). Retrieved

from `https://doi.org/10.1029/2021gl093804` doi: 10.1029/2021gl093804

Jeevanjee, N., & Romps, D. M. (2013, March). Convective self-aggregation, cold pools, and domain size. *Geophysical Research Letters*, *40*(5), 994–998. Retrieved from `https://doi.org/10.1002/grl.50204` doi: 10.1002/grl.50204

Johnson, R. H., Rickenbach, T. M., Rutledge, S. A., Ciesielski, P. E., & Schubert, W. H. (1999, August). Trimodal characteristics of tropical convection. *Journal of Climate*, *12*(8), 2397–2418. Retrieved from `https://doi.org/10.1175/1520-0442(1999)012<2397:tcotc>2.0.co;2` doi: 10.1175/1520-0442(1999)012⟨2397:tcotc⟩2.0.co;2

Khain, A. P., BenMoshe, N., & Pokrovsky, A. (2008, June). Factors determining the impact of aerosols on surface precipitation from clouds: An attempt at classification. *Journal of the Atmospheric Sciences*, *65*(6), 1721–1748. Retrieved from `https://doi.org/10.1175/2007jas2515.1` doi: 10.1175/2007jas2515.1

Khairoutdinov, M. F., & Emanuel, K. (2018, December). Intraseasonal variability in a cloud-permitting near-global equatorial aquaplanet model. *Journal of the Atmospheric Sciences*, *75*(12), 4337–4355. Retrieved from `https://doi.org/10.1175/jas-d-18-0152.1` doi: 10.1175/jas-d-18-0152.1

Kiladis, G. N., Wheeler, M. C., Haertel, P. T., Straub, K. H., & Roundy, P. E. (2009, April). Convectively coupled equatorial waves. *Reviews of Geophysics*, *47*(2). Retrieved from `https://doi.org/10.1029/2008rg000266` doi: 10.1029/2008rg000266

Kim, D., Kug, J.-S., & Sobel, A. H. (2014, January). Propagating versus nonpropagating madden–julian oscillation events. *Journal of Climate*, *27*(1), 111–125. Retrieved from `https://doi.org/10.1175/jcli-d-13-00084.1` doi: 10.1175/jcli-d-13-00084.1

Koren, I., Feingold, G., & Remer, L. A. (2010, September). The invigoration of deep convective clouds over the atlantic: aerosol effect, meteorology or retrieval artifact? *Atmospheric Chemistry and Physics*, *10*(18), 8855–8872. Retrieved from `https://doi.org/10.5194/acp-10-8855-2010` doi: 10.5194/acp-10-8855-2010

Koren, I., Martins, J. V., Remer, L. A., & Afargan, H. (2008, August). Smoke invigoration versus inhibition of clouds over the amazon. *Science*, *321*(5891), 946–949. Retrieved from `https://doi.org/10.1126/science.1159185` doi: 10.1126/science.1159185

Lau, K.-H., & Lau, N.-C. (1990, September). Observed structure and propagation characteristics of tropical summertime synoptic scale disturbances. *Monthly Weather Review*, *118*(9), 1888–1913. Retrieved from `https://doi.org/10.1175/1520-0493(1990)118<1888:osapco>2.0.co;2` doi: 10.1175/1520-0493(1990)118⟨1888:osapco⟩2.0.co;2

Lebo, Z. (2018, February). A numerical investigation of the potential effects of aerosol-induced warming and updraft width and slope on updraft intensity in deep convective clouds. *Journal of the Atmospheric Sciences*, *75*(2), 535–554. Retrieved from `https://doi.org/10.1175/jas-d-16-0368.1` doi: 10.1175/jas-d-16-0368.1

Ling, J., Zhang, C., Joyce, R., ping Xie, P., & Chen, G. (2019, March). Possible role of the diurnal cycle in land convection in the barrier effect on the MJO by the maritime continent. *Geophysical Research Letters*, *46*(5), 3001–3011. Retrieved from `https://doi.org/10.1029/2019gl081962` doi: 10.1029/2019gl081962

Madden, R. A., & Julian, P. R. (1971, July). Detection of a 40–50 day oscillation in the zonal wind in the tropical pacific. *Journal of the Atmospheric Sciences*, *28*(5), 702–708. Retrieved from `https://doi.org/10.1175/1520-0469(1971)028<0702:doadoi>2.0.co;2` doi: 10.1175/1520-0469(1971)028⟨0702:doadoi⟩2.0.co;2

Manabe, S., & Strickler, R. F. (1964, July). Thermal equilibrium of the atmosphere with a convective adjustment. *Journal of the Atmospheric Sciences*, *21*(4), 361–385. Retrieved from `https://doi.org/10.1175/1520-0469(1964)021<0361:teotaw>2.0.co;2` doi: 10.1175/1520-0469(1964)021⟨0361:teotaw⟩2.0.co;2

Mapes, B. E., Chung, E. S., Hannah, W. M., Masunaga, H., Wimmers, A. J., & Velden, C. S. (2018, January). The meandering margin of the meteorological moist tropics. *Geophysical Research Letters*, *45*(2), 1177–1184. Retrieved from `https://doi.org/10.1002/2017gl076440` doi: 10.1002/2017gl076440

Matsugishi, S., & Satoh, M. (2022, May). Sensitivity of the horizontal scale of convective self-aggregation to sea surface temperature in radiative convective equilibrium experiments using a global nonhydrostatic model. *Journal of Advances in Modeling Earth Systems*, *14*(5). Retrieved from `https://doi.org/10.1029/2021ms002636` doi: 10.1029/2021ms002636

Morrison, H., & Grabowski, W. W. (2007, August). Comparison of bulk and bin warm-rain microphysics models using a kinematic framework. *Journal of the Atmospheric Sciences*, *64*(8), 2839–2861. Retrieved from `https://doi.org/10.1175/jas3980` doi: 10.1175/jas3980

Morrison, H., & Grabowski, W. W. (2008, March). Modeling supersaturation and subgrid-scale mixing with two-moment bulk warm microphysics. *Journal of the Atmospheric Sciences*, *65*(3), 792–812. Retrieved from `https://doi.org/10.1175/2007jas2374.1` doi: 10.1175/2007jas2374.1

Morrison, H., & Grabowski, W. W. (2011, October). Cloud-system resolving model simulations of aerosol indirect effects on tropical deep convection and its thermodynamic environment. *Atmospheric Chemistry and Physics*, *11*(20), 10503–10523. Retrieved from `https://doi.org/10.5194/acp-11-10503-2011` doi: 10.5194/acp-11-10503-2011

Morrison, H., & Milbrandt, J. A. (2015, January). Parameterization of cloud microphysics based on the prediction of bulk ice particle properties. part i: Scheme description and idealized tests. *Journal of the Atmospheric Sciences*, *72*(1), 287–311. Retrieved from `https://doi.org/10.1175/jas-d-14-0065.1` doi: 10.1175/jas-d-14-0065.1

Moseley, C., Berg, P., & Haerter, J. O. (2013, dec). Probing the precipitation life cycle by iterative rain cell tracking. *Journal of Geophysical Research: Atmospheres*, *118*(24), 13,361–13,370. Retrieved from `https://doi.org/10.1002%2F2013jd020868` doi: 10.1002/2013jd020868

Muller, C., Yang, D., Craig, G., Cronin, T., Fildier, B., Haerter, J. O., ... Sherwood, S. C. (2022, January). Spontaneous aggregation of convective storms. *Annual Review of Fluid Mechanics*, *54*(1), 133–157. Retrieved from `https://doi.org/10.1146/annurev-fluid-022421-011319` doi: 10.1146/annurev-fluid-022421-011319

Muller, C. J., & Held, I. M. (2012, August). Detailed investigation of the self-aggregation of convection in cloud-resolving simulations. *Journal of the Atmospheric Sciences*, *69*(8), 2551–2565. Retrieved from `https://doi.org/10.1175/jas-d-11-0257.1` doi: 10.1175/jas-d-11-0257.1

Neelin, J. D., & Held, I. M. (1987, January). Modeling tropical convergence based on the moist static energy budget. *Monthly Weather Review*, *115*(1), 3–12. Retrieved from `https://doi.org/10.1175/1520-0493(1987)115<0003:mtcbot>2.0.co;2` doi: 10.1175/1520-0493(1987)115⟨0003:mtcbot⟩2.0.co;2

Neelin, J. D., Peters, O., & Hales, K. (2009, August). The transition to strong convection. *Journal of the Atmospheric Sciences*, *66*(8), 2367–2384. Retrieved from `https://doi.org/10.1175/2009jas2962.1` doi: 10.1175/2009jas2962.1

Nishant, N., & Sherwood, S. C. (2017, June). A cloud-resolving model study of aerosol-cloud correlation in a pristine maritime environment. *Geophysical Research Letters*, *44*(11), 5774–5781. Retrieved from `https://doi.org/10.1002/2017gl073267` doi: 10.1002/2017gl073267

Nishant, N., Sherwood, S. C., & Geoffroy, O. (2019, September). Aerosol-induced modification of organised convection and top-of-atmosphere radiation. *npj Climate and Atmospheric Science*, *2*(1). Retrieved from `https://doi.org/10.1038/s41612-019-0089-1` doi: 10.1038/s41612-019-0089-1

Niu, F., & Li, Z. (2012, September). Systematic variations of cloud top temperature and precipitation rate with aerosols over the global tropics. *Atmospheric Chemistry and Physics*, *12*(18), 8491–8498. Retrieved from `https://doi.org/10.5194/acp-12-8491-2012` doi: 10.5194/acp-12-8491-2012

Nugent, J. M., Turbeville, S. M., Bretherton, C. S., Blossey, P. N., & Ackerman, T. P. (2022, February). Tropical cirrus in global storm-resolving models: 1. role of deep convection. *Earth and Space Science*, *9*(2). Retrieved from `https://doi.org/10.1029/2021ea001965` doi: 10.1029/2021ea001965

Pan, Z., Rosenfeld, D., Zhu, Y., Mao, F., Gong, W., Zang, L., & Lu, X. (2021, May). Observational quantification of aerosol invigoration for deep convective cloud lifecycle properties based on geostationary satellite. *Journal of Geophysical Research: Atmospheres*, *126*(9). Retrieved from `https://doi.org/10.1029/2020jd034275` doi: 10.1029/2020jd034275

Patrizio, C. R., & Randall, D. A. (2019, July). Sensitivity of convective self-aggregation to domain size. *Journal of Advances in Modeling Earth Systems*, *11*(7), 1995–2019. Retrieved from `https://doi.org/10.1029/2019ms001672` doi: 10.1029/2019ms001672

Pendergrass, A. G., Reed, K. A., & Medeiros, B. (2016, November). The link between extreme precipitation and convective organization in a warming climate: Global radiative-convective equilibrium simulations. *Geophysical Research Letters*, *43*(21). Retrieved from `https://doi.org/10.1002/2016gl071285` doi: 10.1002/2016gl071285

Peters, J. M., Lebo, Z. J., Chavas, D. R., & Su, C.-Y. (2023, June). Entrainment makes pollution more likely to weaken deep convective updrafts than invigorate them. *Geophysical Research Letters*, *50*(12). Retrieved from `https://doi.org/10.1029/2023gl103314` doi: 10.1029/2023gl103314

Peters, J. M., Mulholland, J. P., & Chavas, D. R. (2022, March). Generalized lapse rate formulas for use in entraining CAPE calculations. *Journal of the Atmospheric Sciences*, *79*(3), 815–836. Retrieved from `https://doi.org/10.1175/jas-d-21-0118.1` doi: 10.1175/jas-d-21-0118.1

Peters, O., & Neelin, J. D. (2006, May). Critical phenomena in atmospheric precipitation. *Nature Physics*, *2*(6), 393–396. Retrieved from `https://doi.org/10.1038/nphys314` doi: 10.1038/nphys314

Popke, D., Stevens, B., & Voigt, A. (2013, January). Climate and climate change in a radiative-convective equilibrium version of ECHAM6. *Journal of Advances in Modeling Earth Systems*, *5*(1), 1–14. Retrieved from `https://doi.org/10.1029/2012ms000191` doi: 10.1029/2012ms000191

Posselt, D. J., van den Heever, S. C., & Stephens, G. L. (2008, April). Trimodal cloudiness and tropical stable layers in simulations of radiative convective equilibrium. *Geophysical Research Letters*, *35*(8). Retrieved from `https://doi.org/10.1029/2007gl033029` doi: 10.1029/2007gl033029

Reid, J. S., Xian, P., Hyer, E. J., Flatau, M. K., Ramirez, E. M., Turk, F. J., … Maloney, E. D. (2012, February). Multi-scale meteorological conceptual analysis of observed active fire hotspot activity and smoke optical depth in the maritime continent. *Atmospheric Chemistry and Physics*, *12*(4), 2117–2147. Retrieved from `https://doi.org/10.5194/acp-12-2117-2012` doi: 10.5194/acp-12-2117-2012

Roh, W., Satoh, M., & Hohenegger, C. (2021). Intercomparison of cloud properties in DYAMOND simulations over the atlantic ocean. *Journal of the Meteorological Society of Japan. Ser. II*, *99*(6), 1439–1451. Retrieved from `https://doi.org/10.2151/jmsj.2021-070` doi: 10.2151/jmsj.2021-070

Romps, D. M., Latimer, K., Zhu, Q., Jurkat-Witschas, T., Mahnke, C., Prabhakaran, T., … Wendisch, M. (2023, January). Air pollution unable to intensify storms via warm-phase invigoration. *Geophysical Research Letters*, *50*(2). Retrieved from `https://doi.org/10.1029/2022gl100409` doi: 10.1029/2022gl100409

Rosenfeld, D. (1999, October). TRMM observed first direct evidence of smoke from forest fires inhibiting rainfall. *Geophysical Research Letters*, *26*(20), 3105–3108. Retrieved from `https://doi.org/10.1029/1999gl006066` doi: 10.1029/1999gl006066

Rosenfeld, D., Lohmann, U., Raga, G. B., O'Dowd, C. D., Kulmala, M., Fuzzi, S., … Andreae, M. O. (2008, September). Flood or drought: How do aerosols affect precipitation? *Science*, *321*(5894), 1309–1313. Retrieved from `https://doi.org/10.1126/science.1160606` doi: 10.1126/science.1160606

Rotunno, R., Klemp, J. B., & Weisman, M. L. (1988, February). A theory for strong, long-lived squall lines. *Journal of the Atmospheric Sciences*, *45*(3), 463–485. Retrieved from `https://doi.org/10.1175/1520-0469(1988)045<0463:atfsll>2.0.co;2` doi: 10.1175/1520-0469(1988)045⟨0463:atfsll⟩2.0.co;2

Salinas, S. V., Chew, B. N., Miettinen, J., Campbell, J. R., Welton, E. J., Reid, J. S., … Liew, S. C. (2013, March). Physical and optical characteristics of the october 2010 haze event over singapore: A photometric and lidar analysis. *Atmospheric Research*, *122*, 555–570. Retrieved from `https://doi.org/10.1016/j.atmosres.2012.05.021` doi: 10.1016/j.atmosres.2012.05.021

Shpund, J., Khain, A., & Rosenfeld, D. (2019, August). Effects of sea spray on microphysics and intensity of deep convective clouds under strong winds. *Journal of Geophysical Research: Atmospheres*, *124*(16), 9484–9509. Retrieved from `https://doi.org/10.1029/2018jd029893` doi: 10.1029/2018jd029893

Singh, M. S., & O'Gorman, P. A. (2013, August). Influence of entrainment on the thermal stratification in simulations of radiative-convective equilibrium. *Geophysical Research Letters*, *40*(16), 4398–4403. Retrieved from `https://doi.org/10.1002/grl.50796` doi: 10.1002/grl.50796

Singh, M. S., & O'Gorman, P. A. (2015, June). Increases in moist-convective updraught velocities with warming in radiative-convective equilibrium. *Quarterly Journal of the Royal Meteorological Society*, *141*(692), 2828–2838. Retrieved from `https://doi.org/10.1002/qj.2567` doi: 10.1002/qj.2567

Sobel, A. H., Nilsson, J., & Polvani, L. M. (2001, December). The weak temperature gradient approximation and balanced tropical moisture waves. *Journal of the Atmospheric Sciences*, *58*(23), 3650–3665. Retrieved from `https://doi.org/10.1175/1520-0469(2001)058<3650:twtgaa>2.0.co;2` doi: 10.1175/1520-0469(2001)058⟨3650:twtgaa⟩2.0.co;2

Stevens, B., Satoh, M., Auger, L., Biercamp, J., Bretherton, C. S., Chen, X., … Zhou, L. (2019, September). DYAMOND: the DYnamics of the atmospheric general circulation modeled on non-hydrostatic domains. *Progress in Earth and Planetary Science*, *6*(1). Retrieved from `https://doi.org/10.1186/s40645-019-0304-z` doi: 10.1186/s40645-019-0304-z

Storer, R. L., & van den Heever, S. C. (2013, February). Microphysical processes evident in aerosol forcing of tropical deep convective clouds. *Journal of the Atmospheric Sciences*, *70*(2), 430–446. Retrieved from `https://doi.org/10.1175/jas-d-12-076.1` doi: 10.1175/jas-d-12-076.1

Storer, R. L., van den Heever, S. C., & L'Ecuyer, T. S. (2014, April). Observations of aerosol-induced convective invigoration in the tropical east atlantic. *Journal of Geophysical Research: Atmospheres*, *119*(7), 3963–3975. Retrieved from `https://doi.org/10.1002/2013jd020272` doi: 10.1002/2013jd020272

Su, C.-Y., Chen, W.-T., Wu, C.-M., & Ma, H.-Y. (2022). Object-based evaluation of tropical precipitation systems in DYAMOND simulations over the maritime continent. *Journal of the Meteorological Society of Japan. Ser. II*, *100*(4), 647–659. Retrieved from https://doi.org/10.2151/jmsj.2022-033 doi: 10.2151/jmsj.2022-033

Su, C.-Y., Wu, C.-M., Chen, W.-T., & Chen, J.-H. (2021a, July). The effects of the unified parameterization in the CWBGFS: the diurnal cycle of precipitation over land in the maritime continent. *Climate Dynamics*, *58*(1-2), 223–233. Retrieved from https://doi.org/10.1007/s00382-021-05899-2 doi: 10.1007/s00382-021-05899-2

Su, C.-Y., Wu, C.-M., Chen, W.-T., & Chen, J.-H. (2021b, October). Implementation of the unified representation of deep moist convection in the CWBGFS. *Monthly Weather Review*, *149*(10), 3525–3539. Retrieved from https://doi.org/10.1175/mwr-d-21-0067.1 doi: 10.1175/mwr-d-21-0067.1

Tao, W.-K., Chen, J.-P., Li, Z., Wang, C., & Zhang, C. (2012, April). Impact of aerosols on convective clouds and precipitation. *Reviews of Geophysics*, *50*(2). Retrieved from https://doi.org/10.1029/2011rg000369 doi: 10.1029/2011rg000369

Tomassini, L. (2020, August). The interaction between moist convection and the atmospheric circulation in the tropics. *Bulletin of the American Meteorological Society*, *101*(8), E1378–E1396. Retrieved from https://doi.org/10.1175/bams-d-19-0180.1 doi: 10.1175/bams-d-19-0180.1

Tsai, W.-M., & Wu, C.-M. (2017, September). The environment of aggregated deep convection. *Journal of Advances in Modeling Earth Systems*, *9*(5), 2061–2078. Retrieved from https://doi.org/10.1002/2017ms000967 doi: 10.1002/2017ms000967

Turbeville, S. M., Nugent, J. M., Ackerman, T. P., Bretherton, C. S., & Blossey, P. N. (2022, February). Tropical cirrus in global storm-resolving models: 2. cirrus life cycle and top-of-atmosphere radiative fluxes. *Earth and Space Science*, *9*(2). Retrieved from https://doi.org/10.1029/2021ea001978 doi: 10.1029/2021ea001978

van den Heever, S. C., & Cotton, W. R. (2007, June). Urban aerosol impacts on downwind convective storms. *Journal of Applied Meteorology and Climatology*, *46*(6), 828–850. Retrieved from https://doi.org/10.1175/jam2492.1 doi: 10.1175/jam2492.1

van den Heever, S. C., Stephens, G. L., & Wood, N. B. (2011, April). Aerosol indirect effects on tropical convection characteristics under conditions of radiative–convective equilibrium. *Journal of the Atmospheric Sciences*, *68*(4), 699–718. Retrieved from https://doi.org/10.1175/2010jas3603.1 doi: 10.1175/2010jas3603.1

Varble, A. (2018, April). Erroneous attribution of deep convective invigoration to aerosol concentration. *Journal of the Atmospheric Sciences*, *75*(4), 1351–1368. Retrieved from https://doi.org/10.1175/jas-d-17-0217.1 doi: 10.1175/jas-d-17-0217.1

Windmiller, J. M., & Hohenegger, C. (2019, December). Convection on the edge. *Journal of Advances in Modeling Earth Systems*, *11*(12), 3959–3972. Retrieved from https://doi.org/10.1029/2019ms001820 doi: 10.1029/2019ms001820

Wing, A. A., Emanuel, K., Holloway, C. E., & Muller, C. (2017, February). Convective self-aggregation in numerical simulations: A review. *Surveys in Geophysics*, *38*(6), 1173–1197. Retrieved from https://doi.org/10.1007/s10712-017-9408-4 doi: 10.1007/s10712-017-9408-4

Wing, A. A., & Emanuel, K. A. (2014, February). Physical mechanisms controlling self-aggregation of convection in idealized numerical modeling simulations. *Journal of Advances in Modeling Earth Systems*, *6*(1), 59–74. Retrieved from https://doi.org/10.1002/2013ms000269 doi: 10.1002/2013ms000269

Wing, A. A., Reed, K. A., Satoh, M., Stevens, B., Bony, S., & Ohno, T. (2018, March). Radiative–convective equilibrium model intercomparison project.

Geoscientific Model Development, *11*(2), 793–813. Retrieved from https://doi.org/10.5194/gmd-11-793-2018 doi: 10.5194/gmd-11-793-2018

Wing, A. A., Stauffer, C. L., Becker, T., Reed, K. A., Ahn, M.-S., Arnold, N. P., ... Zhao, M. (2020, September). Clouds and convective self-aggregation in a multimodel ensemble of radiative-convective equilibrium simulations. *Journal of Advances in Modeling Earth Systems*, *12*(9). Retrieved from https://doi.org/10.1029/2020ms002138 doi: 10.1029/2020ms002138

Wu, C.-M., & Arakawa, A. (2014, May). A unified representation of deep moist convection in numerical modeling of the atmosphere. part II. *Journal of the Atmospheric Sciences*, *71*(6), 2089–2103. Retrieved from https://doi.org/10.1175/jas-d-13-0382.1 doi: 10.1175/jas-d-13-0382.1

Yanase, T., Nishizawa, S., Miura, H., & Tomita, H. (2022, September). Characteristic form and distance in high-level hierarchical structure of self-aggregated clouds in radiative-convective equilibrium. *Geophysical Research Letters*, *49*(18). Retrieved from https://doi.org/10.1029/2022gl100000 doi: 10.1029/2022gl100000

Yang, G.-Y., & Slingo, J. (2001, April). The diurnal cycle in the tropics. *Monthly Weather Review*, *129*(4), 784–801. Retrieved from https://doi.org/10.1175/1520-0493(2001)129<0784:tdcitt>2.0.co;2 doi: 10.1175/1520-0493(2001)129⟨0784:tdcitt⟩2.0.co;2

Zhang, C., & Ling, J. (2017, May). Barrier effect of the indo-pacific maritime continent on the MJO: Perspectives from tracking MJO precipitation. *Journal of Climate*, *30*(9), 3439–3459. Retrieved from https://doi.org/10.1175/jcli-d-16-0614.1 doi: 10.1175/jcli-d-16-0614.1

Modulation of Tropical Convection-circulation Interaction by Aerosol Indirect Effects in Idealized Simulations of a Global Convection-permitting Model

Chun-Yian Su[1,2], Chien-Ming Wu[2], Wei-Ting Chen[2], and John M. Peters[1]

[1]Department of Meteorology and Atmospheric Science, The Pennsylvania State University, University Park, PA
[2]Department of Atmospheric Sciences, National Taiwan University, Taipei city, Taiwan

Key Points:

- Tropical convection, large-scale circulation, and their responses to pollution are physical processes that couple together.
- Pollution leads to weaker large-scale circulation, the closeness of convection to the moist cluster edges, and more mid-level cloud water.
- Pollution facilitates deep convection development in a drier environment but reduces large-scale instability and convection intensity.

Corresponding author: Chun-Yian Su, `czs6237@psu.edu`

Abstract

Observations suggest tropical convection intensifies when aerosol concentrations enhance, but quantitative estimations of this effect remain highly uncertain. Leading theories for explaining the influence of aerosol concentrations on tropical convection are based on the dynamical response of convection to changes in cloud microphysics, neglecting possible changes in the environment. In recent years, global convection-permitting models (GCPM) have been developed to circumvent problems arising from imposing artificial scale separation on physical processes associated with deep convection. Here, we use a GCPM to investigate how enhanced concentrations of aerosols that act as cloud condensate nuclei (CCN) impact tropical convection features by modulating the convection-circulation interaction. Results from a pair of idealized non-rotating radiative-convective equilibrium simulations show that the enhanced CCN concentration leads to weaker large-scale circulation, the closeness of deep convective systems to the moist cluster edges, and more mid-level cloud water at an equilibrium state in which convective self-aggregation occurred. Correspondingly, the enhanced CCN concentration modulates how the diabatic processes that support or oppose convective aggregation maintain the aggregated state at equilibrium. Overall, the enhanced CCN concentration facilitates the development of deep convection in a drier environment but reduces the large-scale instability and the convection intensity. Our results emphasize the importance of allowing atmospheric phenomena to evolve continuously across spatial and temporal scales in simulations when investigating the response of tropical convection to changes in cloud microphysics.

Plain Language Summary

How does air pollution affect thunderstorm intensity over the tropical ocean? Past studies have proposed different opinions but generally neglect the interplay between the development of thunderstorms and the long-range movement of air that redistributes the Earth's thermal energy and moisture. Here, we address this question by investigating results from idealized numerical experiments in which the global domain is used to simultaneously simulate the response of individual thunderstorms and large-scale air motion to pollution. We found that pollution makes the thunderstorms keep less moisture in their surroundings, limiting the intensity of thunderstorms and weakening the large-scale air motion that supplies moisture to thunderstorms. Our results suggest that the interplay between the development of thunderstorms and the long-range movement of air is crucial in determining the effects of pollution in the tropical atmosphere.

1 Introduction

Tropical moist convection has long been recognized as a critical role in the global climate system (Arakawa, 2004; Hartmann et al., 2001). Various meteorological phenomena in the tropics are associated with the interaction between moist convection and atmospheric circulation, such as mesoscale convective systems (Houze, 2004) and convectively coupled waves (Kiladis et al., 2009; Lau & Lau, 1990). A deeper understanding of convection-circulation interaction across temporal and spatial scales is important for improving global climate predictions and forecasts of extreme precipitation events (Tomassini, 2020).

In recent years, several numerical modeling groups have developed global convection-permitting models (GCPMs) that explicitly simulate deep moist convection on the global domain to circumvent problems arising from parameterizations that presumably determine how circulations govern moist convection or how moist convection drives circulations (Caldwell et al., 2021; Hohenegger et al., 2023; Stevens et al., 2019). Interestingly, while the GCPMs capture basic aspects of the general circulation, they produce a diverse range of tropical convective systems (Feng et al., 2023; Su et al., 2022). For example, the distribution of tropical cloud modes varies greatly across the models (Nugent et al., 2022; Roh et al., 2021; Turbeville et al., 2022). The diversity in tropical convection features among the GCPMs has not been fully understood. One of the challenges to closing the knowledge gap is that the response of tropical convection and the large-scale circulation to any model treatment of subgrid-scale physical process (e.g., turbulence, microphysics) or natural and anthropogenic forcing are coupled throughout simulations. Hence, identifying the sensitivity of tropical convection-circulation to individual components or processes in the global climate system is critical to understanding the cause of the diverse tropical convection features among the GCPMs. Observations suggest that enhanced aerosol concentrations that arise from human activities and natural sources can substantially influence updrafts of tropical deep convection (Andreae et al., 2004; Koren et al., 2008; Niu & Li, 2012; Pan et al., 2021; Storer et al., 2014), but leading theories for explaining the influence neglects possible changes in the environment through convection-circulation interaction. In this study, we aim to investigate the impact of enhanced aerosol concentrations on tropical convection features using a GCPM.

By acting as cloud condensate nuclei (CCN) or ice nuclei (IN), aerosols change cloud properties by influencing cloud microphysics and dynamics, meanwhile influencing cloud-radiation feedbacks (i.e., aerosol indirect effects (AIEs); see reviews of Fan et al. (2016) and Tao et al. (2012)). However, the underlying mechanisms of how the updrafts are influenced remain elusive and are often debated (Fan et al., 2018; Fan & Khain, 2021; Grabowski & Morrison, 2020, 2021; Igel & van den Heever, 2021; J. M. Peters et al., 2023; Romps et al., 2023). A particular challenge of understanding AIEs using observations is that the observed aerosol concentrations in the environments of tropical deep convection often covary with other meteorological factors, such as convective available potential energy and vertical wind shear (Grabowski, 2018; Nishant & Sherwood, 2017; Varble, 2018), and the influences of meteorological and aerosol variability are difficult to disentangle from one another. Further, there is evidence from simulations that AIEs on deep convection vary as a function of meteorological conditions such as shear and humidity (Fan et al., 2009; van den Heever & Cotton, 2007; Khain et al., 2008; Koren et al., 2010; Lebo, 2018), which further complicates our ability to isolate the aerosol effects from other meteorological processes.

To take into account the interaction between tropical convection and the surrounding environment, Abbott and Cronin (2021) carried out simulations using a small domain (128x128 km^2) three-dimension cloud-resolving model (3-D CRM) with parameterized large-scale dynamics under the weak temperature gradient (WTG) approximation (Sobel et al., 2001). They suggested that enhanced aerosol concentrations produce clouds that mix more condensed water into the surrounding air. This enhances the environment favorably for subsequent convection by moistening the free troposphere and reducing the deleterious effects of entrainment. The humidity-entrainment mechanism they proposed is distinct from past work, which linked stronger updrafts with latent heat released by cloud condensation (Fan et al., 2018) or freezing (Rosenfeld et al., 2008) independently from possible changes in the environment. Using a similar modeling framework but under a different large-scale flow regime, Anber et al. (2019) found a contrasting result. In their simulations, convection and mean precipitation get weaker when the CCN concentration increases. They suggested that the changes are associated with the modulation of the coupling between convective processes and large-scale motions, which reduces surface enthalpy fluxes, rather than the changes in microphysical properties.

In CRM simulations that use a large domain for explicitly simulating the large-scale circulation between convecting and nonconvecting regions, results of AIEs on tropical convection have not reached a consensus as well. For example, van den Heever et al. (2011) found a weak response of the large-scale organization of convection and the domain-averaged precipitation to enhanced CCN concentrations in their 2-D CRM simulations (10000 km) configured in non-rotating radiative-convective equilibrium (RCE; Manabe & Strickler, 1964) with a fixed sea surface temperature (SST). They suggested that AIEs on the three tropical cloud modes are quite significant in magnitude and often opposite in sign, offsetting each other, thus producing a weak domain-wide response. In contrast, Beydoun and Hoose (2019) found a comparatively large decrease in domain-averaged precipitation with enhanced CCN concentrations in their RCE simulations of a channel-shaped (2000x120 km^2) 3-D CRM. They suggested that enhanced CCN concentrations weaken the large-scale organization of convection, leading to decreased domain-averaged precipitation. As discussed in Beydoun and Hoose (2019), the discrepancy between the results of the two studies may be caused by the difference in how the aerosol changes are imposed and the difference in model setup of domain geometry. Previous studies of RCE simulations found that the size of the simulation domain impacts the mechanisms that trigger and maintain the large-scale organization of convection (Jeevanjee & Romps, 2013; C. J. Muller & Held, 2012; Patrizio & Randall, 2019). A horizontal scale of model domain larger than 5000 km was suggested to be large enough to represent the natural scale of large-scale organization of convection and reach convergence of equilibrium states in simulations with different domain sizes (Matsugishi & Satoh, 2022; Yanase et al., 2022).

The goal of this study is to investigate how enhanced CCN concentration impacts tropical convection features through modulating the convection-circulation interaction using a GCPM that simultaneously simulates the dynamical response of tropical deep convection to changes in cloud microphysics and allows the large-scale organization of convection to naturally develop without artificial constraints due to domain size or shape. Idealized non-rotating RCE simulations with different scenarios of CCN concentration were carried out using the Central Weather Bureau Global Forecast System (CWBGFS; Su et al., 2021a).

Simulations configured in RCE have been extensively used to investigate feedbacks among clouds, environmental moisture, radiation, and precipitation (Bretherton et al., 2005; Coppin & Bony, 2015; Cronin & Wing, 2017; K. Emanuel et al., 2014; Holloway & Woolnough, 2016; Pendergrass et al., 2016; Popke et al., 2013; Singh & O'Gorman, 2013, 2015; Wing & Emanuel, 2014; Wing et al., 2020), providing an ideal experimental setting for our study. Previous studies found that convection in simulations configured in RCE can spontaneously self-organize into one or more moist ascending clusters surrounded by dry subsiding convection-free areas (convective self-aggregation (CSA); C. Muller et al., 2022; Wing et al., 2017). The occurrence of CSA changes the climate mean state dramatically (i.e., atmospheric heating and drying) and gives rise to the large-scale organization of convection that develops in line with the large-scale circulation. As will be shown later in this paper, CSA occurs in both of our simulations, but the degree of large-scale organization of convection changes with the enhancement of CCN concentration. We note that the terminologies of large-scale organization of convection and aggregation are used interchangeably in this paper, as they represent the same concept, at least in the scope of this study. The following section introduces more details about the model and our experiment design. Section 3 describes the results of the simulations when a statistical equilibrium is reached, and the summary and discussion are presented in section 4.

2 Model Description and Experiment Design

The Central Weather Bureau Global Forecast System (CWBGFS; Su et al., 2021a) is a global convection-permitting model that run at the horizontal resolution of around 15 km. Deep convection in the CWBGFS is represented by the unified relaxed Arakawa-Schubert scheme (URAS; Su et al., 2021b) in which the representation transitions from the parameterization to the explicit simulation as the diagnosed convective updraft fraction increases (Arakawa & Wu, 2013; Wu & Arakawa, 2014). Hence, the CWBGFS with the URAS can explicitly but efficiently simulate deep convection and the associated convection-circulation interaction on a global scale. The model partially resolves circulations in organized convective systems and reproduces the observed feature of convective systems that stronger extreme precipitation occurs in horizontally larger systems (Su et al., 2022).

In the CWBGFS, cloud microphysical processes, including cloud droplet activation, are represented by the two-moment Predicted Particle Properties bulk microphysics scheme (P3; Morrison & Milbrandt, 2015). Since the convective updraft fraction increases with updraft velocity so that the representation of deep convection transitions to explicit simulation as updraft enhances (Su et al., 2021b), we assume that taking cloud-aerosol interaction into account in the cloud model of URAS makes a small impact on the tropical convection features and will not change the conclusion of this study. On average, more than 93 % of precipitation is produced by explicitly simulated convection through the P3 scheme over precipitation events stronger than 5 mm h^{-1}. In the version of the P3 scheme used in this study, the aerosol is specified as a lognormal size distribution with a constant background aerosol concentration and mean size of 0.05 μm, consisting of ammonium sulfate. The number of activated CCN is a function of supersaturation given by Morrison and Grabowski (2007, 2008). The rest of the descriptions regarding physics suites and the dynamic core of the CWBGFS can be found in Su et al. (2021a).

We carried out two idealized non-rotating aqua-planet simulations configured in RCE with different constant background aerosol concentrations using the CWBGFS. Setting the background aerosol concentration as a constant provides us the simplest scenario for examining the changes in convection variability over space and the pattern of large-scale circulation with aerosol concentrations. As this study focuses on the AIEs, aerosols in the microphysics scheme do not interact with radiation. The current study sets the constant background aerosol concentration to 3x10^{8} kg^{-1} (pristine run) and 3x10^{10} kg^{-1} (polluted run) throughout the simulation, respectively. The scenarios here are referred to the marine environment (Andreae, 2009) and the urban environment (Chang et al., 2021). Previous studies suggested that tropical mean precipitation does not change with the enhancement of CCN concentration monotonically (van den Heever et al., 2011; Storer & van den Heever, 2013). Experiments with more diverse polluted scenarios will be carried out in the future.

The pristine run and the polluted run are initialized with the same analytic sounding (Wing et al., 2018) that approximates the moist tropical sounding of Dunion (2011), and the initial horizontal winds are set to zero. The initial surface pressure of all grid columns is 1014.8 hPa. The incoming solar radiation (409.6 W m^{-2}), the SST (300 K), and the surface albedo (0.07) are spatially uniform and remain constant in time. The simulations are run for 120 days, and the random perturbation of temperature from 0.1 to 0.02 K is added to the five lowest model levels in the first 20 days to speed up convection initiation. In the following section, we analyze results from day 100 to 120 when a statistical equilibrium state is met (Fig. S1) using hourly outputs. We note that the two runs may experience different transition processes to arrive at their equilibrium state, and a slow-phase oscillation of the global energy budget could exist. We assume that the probable presence of such a slow-phase oscillation would not change the conclusion of this study because the energy budget in both runs does not exhibit an obvious changing trend in the last 50 days of integration (Fig. S1).

3 Results

The RCE simulations in this study have typical features of CSA shown in the global model simulations of the RCE model intercomparison project (Wing et al., 2018, 2020), showing drying of the atmosphere and enhancement of spatial moisture variance. As convection self-organizing into multiple moist clusters, the global average of CWV decreases from the initial condition of 49.93 mm to the equilibrium state (day 100-120) of 29.96 mm in the pristine run and 29.73 mm in the polluted run (Fig. S1). Fig. 1 shows the spatial distribution of CWV at day 110. Both runs exhibit a high heterogeneity of CWV within moist clusters, which is coupled to convection. The pristine run has notably more occurrence of high CWV events (>60 mm). One can see that the CWV hotspots (>60 mm) in the pristine run occur over regions closer to the geometric center of each moist cluster than they do in the polluted run. We find that this particular feature may play an important role in the convection-circulation interaction, which will be investigated later in this paper.

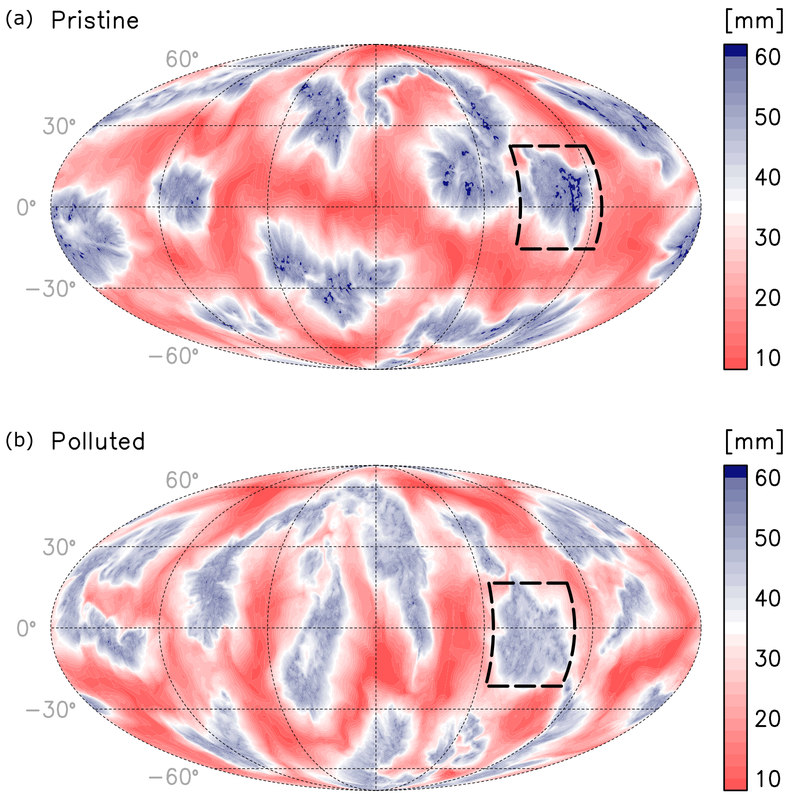

Figure 1. Spatial distribution of CWV at day 110 of the pristine run (a) and the polluted run (b).

At the equilibrium state, both runs exhibit a bimodal probability distribution of CWV (Fig. 2). The bimodality is associated with the presence of an aggregated state of convection (Tsai & Wu, 2017). The difference in CWV between the two local maxima of the bimodality is smaller in the polluted run, suggesting that the aggregated state in the polluted run is maintained by weaker large-scale circulation, and the aggregated state consists of drier moist clusters and wetter dry regions. Associated with the weakened large-scale circulation, the global averages of outward OLR and precipitation intensity at the equilibrium state are lower in the polluted run (287.45 W m^{-2}, 0.167 mm h^{-1}) than that in the pristine run (292.43 W m^{-2}, 0.174 mm h^{-1}). The polluted run has a colder temperature profile compared to that in the pristine run, with the largest difference of 1.7 K occurring at 200 hPa (Fig. S2). Meanwhile, the polluted run has the lower spatial variance of vertically integrated frozen moist static energy (FMSE) (1.03×10^{15} $J^2 m^{-4}$) compared to that in the pristine run (1.32×10^{15} $J^2 m^{-4}$). The FMSE has been used in studies of CSA to quantify the degree of aggregation

$$h = C_pT + gz + L_vq_v - L_fq_{ice}, \tag{1}$$

where C_p is the specific heat capacity of air, T is temperature, g is the gravitational acceleration, z is geopotential height, L_v is the latent heat of vaporization, q_v is the water vapor mixing ratio, L_f is the latent heat of fusion, and q_{ice} represents all ice phase condensates. During our analysis period, the variation in the spatial variance of vertically integrated FMSE with time in both runs is much less than the difference between the two runs (Fig. S3).

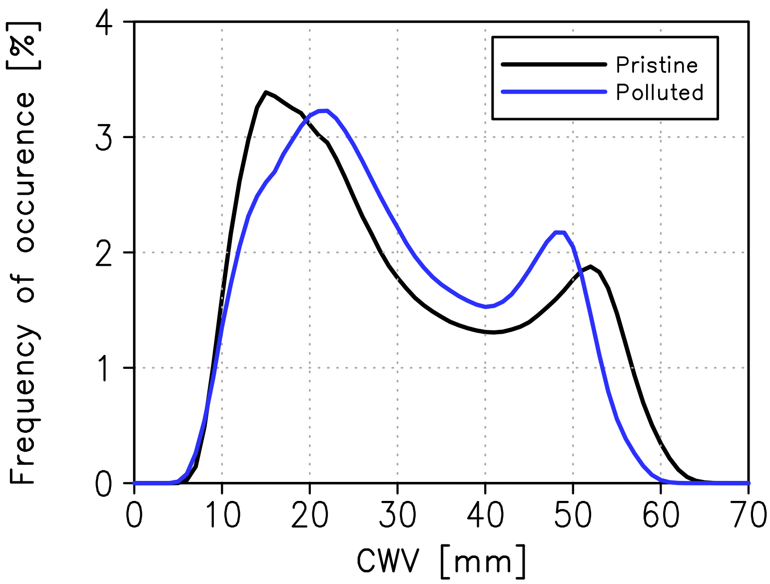

Figure 2. Probability distribution of CWV from days 100 to 120.

To identify the changes in energy transport between moist clusters and dry regions caused by pollution, we use the stream function on moisture space (Arnold & Putman, 2018)

$$\Psi_i(p) = \Psi_{i-1}(p) + \omega_i(p), \tag{2}$$

where p is pressure and ω_i is the pressure velocity averaged over the i^{th} CWV bin. Both runs in this study exhibit a shallow circulation, which transports moist static energy (MSE) upgradient, maintaining the large-scale organization of convection (Arnold & Putman, 2018; C. Muller et al., 2022), and a deep circulation, which exports MSE from moist ascending regions (Fig. 3a and 3b). While the deep circulation is directly driven by deep convection, the differential radiative cooling between moist clusters and dry regions (Fig. 3c and Fig. 3d) associated with the vertical gradients of relative humidity and clouds over dry regions (Fig. 3e and Fig. 3f) is believed to be one of the factors that drive shallow circulation in RCE simulations (C. J. Muller & Held, 2012). In general, the patterns of energy transport in the two runs are very much alike. The polluted run has the larger stream function at the upper free troposphere (300-400 hPa) compared to that in the pristine run (Fig. 3a and 3b), which suggests that the mean ascending motions are distributed wider in the moisture space when the environment is more polluted. However, the difference in the density of the stream function contours over there between the two runs is marginal. The difference in the low-level subsidence over dry regions between the two runs is also hard to be identified through Fig. 3a and 3b. We note that the polluted run has a higher cloud water mixing ratio over grid columns with CWV more than the 70$^{\text{th}}$ percentile compared to that in the pristine run, which is likely caused by enhanced cloud drop activation due to pollution.

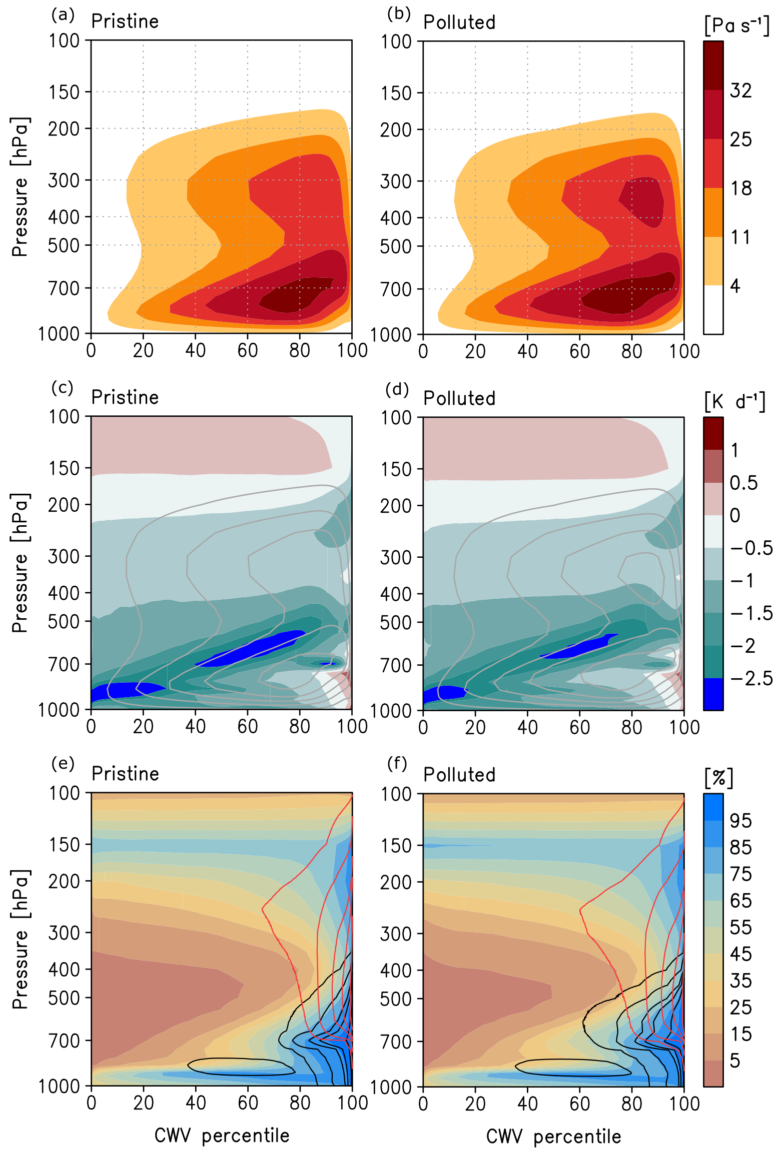

Figure 3. Vertical profiles of stream function (shaded) (a,b), radiative heating rate (shaded) (c,d), relative humidity (shaded), and cloud water (black) and cloud ice (red) mixing ratio contoured at 0.001, 0.01, 0.05, 0.1, 0.3 g kg^{-1} (e,f) conditionally sampled by CWV in the pristine run (left column) and the polluted run (right column) from day 100 to 120. The stream function in a,b is shown as contours in c,d.

As the stream function on moisture space does not represent physical horizontal flows, we further analyze the large-scale circulation on physical space in each run. We define moist clusters as contiguous grid columns with CWV >75$^{\text{th}}$ percentile in horizontal directions and dry regions as areas not defined as moist clusters. The 75$^{\text{th}}$ percentile of CWV is 42.34 mm in the pristine run and 40.75 mm in the polluted run. For each grid column, the distance to the edge of the nearest moist cluster with a spatial scale larger than 500 km (defined as the square root of horizontal area) is calculated. Horizontal winds at each vertical level are then projected to the direction pointing to the nearest edge and conditionally sampled by the distance to the edge. We neglect moist clusters smaller than 500 km because they are rare events that quickly dissipate or merge into larger moist clusters. The distance-binned projected horizontal wind speed and vertical velocity are shown in Fig. 4a and 4b. Negative distance values refer to areas inside the moist clusters as the distance is multiplied by -1 for grid columns belong a moist cluster.

The plot makes it clear that the polluted run has a weaker low-level inflow (below 850 hPa) from dry regions to moist clusters and a weaker high-level outflow (above 300 hPa) compared to those in the pristine run. Over moist clusters, the mean ascending motions are weaker and closer to the edge in the polluted run, but the difference in the maximum magnitude of the mean updrafts between the two runs is subtle. The mean CWV is homogeneous in regions within moist clusters but away from the edge ($d < -500\,km, d = distance\ to\ the\ nearest\ edge$) (Fig. 5a), while the distribution of the mean precipitation intensity is maximized near the edge (Fig. 5b) reflecting the distribution of the mean ascending motions. We speculate that the imprint of the changes in deep convection features caused by pollution on large-scale circulation is illustrated by analysis based on physical space rather than moisture space because the impact of pollution on deep convection intensity does not enhance or reduce monotonically to the increase in CWV.

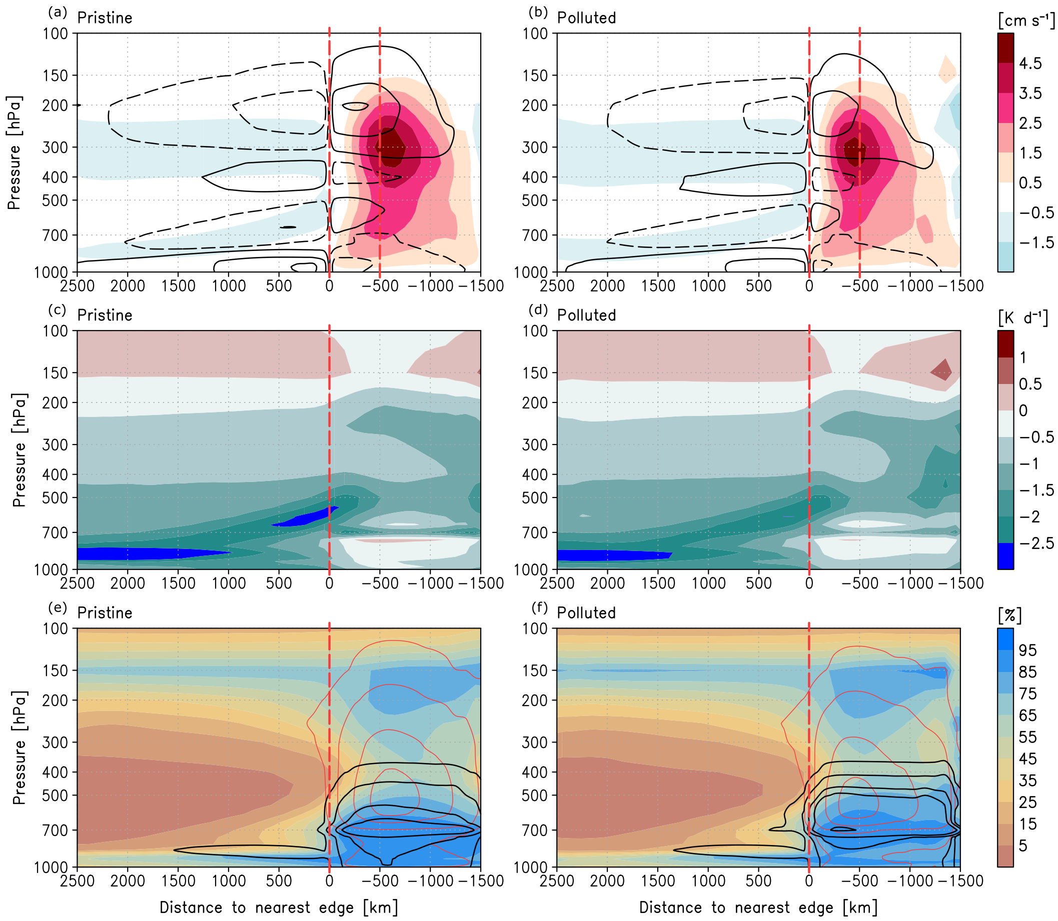

Figure 4. Vertical profiles of projected horizontal wind speed (contours at 0.5, 2.5, 4.5 m s^{-1}), vertical velocity (shaded) (a,b), radiative heating rate (shaded) (c,d), relative humidity (shaded), and cloud water (black) and cloud ice (red) mixing ratio contoured at 0.001, 0.01, 0.05, 0.1, 0.3 g kg^{-1} (e,f) conditionally sampled by the distance to the nearest edge in the pristine run (left column) and the polluted run (right column) from day 100 to 120. Projected horizontal wind pointing toward (away) the edge is shown by solid (dashed) contours. Negative distance values refer to areas inside the moist clusters

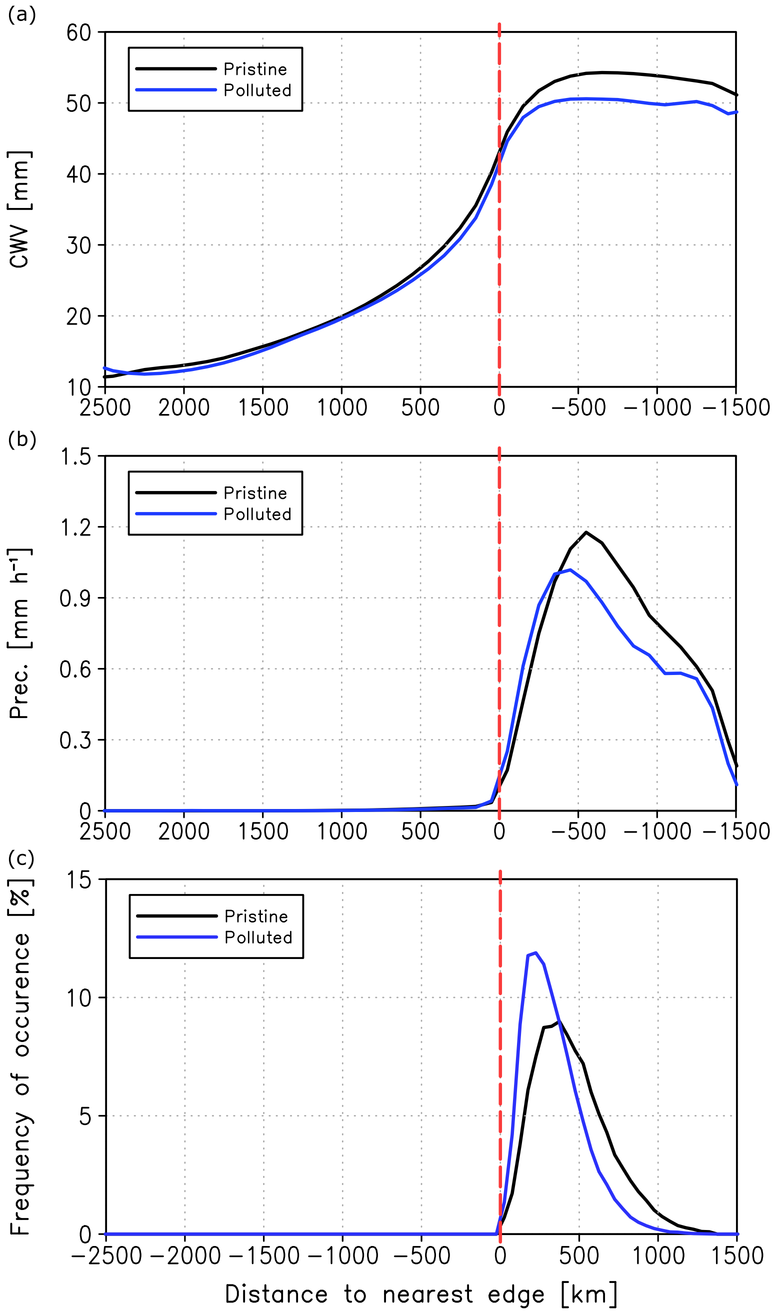

Figure 5. CWV (a), precipitation intensity (b), and the occurrence of explicitly simulated convection objects (c) conditionally sampled by the distance to the nearest edge from day 100 to 120.

We zoom in to one of the moist clusters to showcase the difference in the spatial distribution of convection between the two runs. Fig. 6a-d show the snapshots of vertical velocity at 500 hPa on top of CWV and precipitation intensity within the dashed rectangle shown in Fig. 1. In the polluted run, explicitly simulated convection develops over regions closer to the edge compared to that in the pristine run. This inference is further supported by the analysis of the distance from the geometric center of each convection object to its nearest edge (Fig. 5c), in which a convection object is defined as contiguous grid cells with vertical velocity at 500 hPa >0.1 m s^{-1}. In both runs, the highest probability of convection object occurrence is located at $-500 < d < 0\,km$.

Why are updrafts, especially those in the polluted run, preferably take place close to the edge? Intensification of tropical deep convection at the edge of convectively active regions has been identified by previous studies of observations (Mapes et al., 2018) and idealized RCE simulations (Becker et al., 2018; Windmiller & Hohenegger, 2019). Windmiller and Hohenegger (2019) proposed that the cause for the edge intensification is dynamical lifting by strong surface convergence that results from two opposing flows: a low-level inflow from dry regions to moist clusters and the propagation of continuously forming cold pools within moist clusters. Fig. 6e,f show the spatial distribution of the divergence field at 1000 hPa in our simulations. We can see the near-surface divergence collocates with updrafts, and strong near-surface convergence can be seen at regions between the edge and the existing updrafts. We speculate that the mechanism proposed by Windmiller and Hohenegger (2019) explains the edge intensification in our simulations, and the weaker low-level inflow in the polluted run may be one of the factors to polluted updrafts being closer to the edge. As will be shown later in this paper, pollution has a larger impact on the probability distribution of near-surface inflow than its impact on the probability distribution of the estimated cold pool propagation velocity in our simulations.

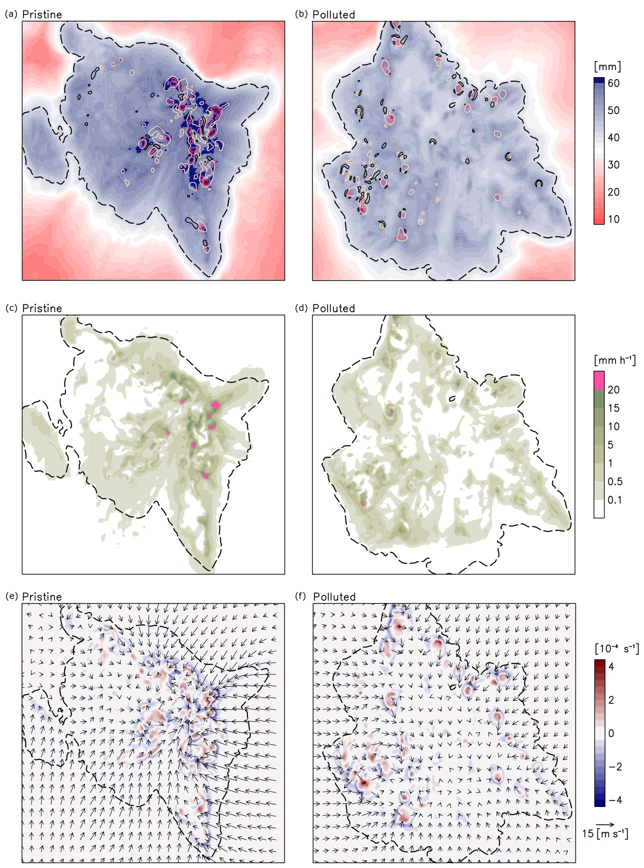

Figure 6. Spatial distribution of CWV, updraft velocity at 500 hPa (red scale, contoured at 0.1, 0.5, 1, 1.5 m s^{-1}), downdraft velocity at 500 hPa (black solid, contoured at 0.1 m s^{-1}) (a,b), precipitation intensity (c,d), and divergence field at 1000 hPa at day 110 of the pristine run (left column) and the polluted run (right column). The edge of the moist cluster (i.e., the 75$^{\text{th}}$ percentile of CWV) is demonstrated by black dashed lines.

Table 1. Spatial and temporal mean of each term in the right-hand side of eq.3

$[day^{-1}]$	Pristine moist clusters	Pristine dry regions	Polluted moist clusters	Polluted dry regions
Advection	-0.060	-0.007	-0.097	-0.004
SEF	-0.069	0.001	-0.045	-0.005
NetLW	0.065	-0.004	0.087	-0.001
NetSW	0.057	0.015	0.049	0.016

The distance-binned radiative heating rate, relative humidity, and hydrometeors mixing ratio over dry regions (Fig. 4c-f) resemble the CWV-binned results (Fig. 3c-f), except in physical space it is apparent that the polluted run has more mid-level (700 hPa) cloud water over the regions close to the edge ($0 < d < 500\,km$) than the pristine run does. The level of the cloud water coincides with the level of the outflow of shallow circulation from moist clusters, suggesting that polluted moist clusters export more cloud water to the dry regions than their pristine counterparts, and pollution may modulate the role of shallow circulation in maintaining the aggregated state.

To investigate the modulation of the diabatic processes that support or oppose convective aggregation by pollution, we analyze a budget of the spatial variance of FMSE at the equilibrium state as a quantitative account of the large-scale organization of convection following (Wing & Emanuel, 2014). The FMSE is a desirable diagnostic because vertically integrated FMSE can only be changed by radiation, surface fluxes, and advection. A process that contributes to the FMSE variance supports aggregation, and a process that reduces the FMSE variance opposes aggregation.

The budget equation of vertically integrated FMSE is given by eq. (9) in Wing and Emanuel (2014)

$$\frac{1}{2}\partial_t \hat{h}'^2 = -\hat{h}'\nabla_h \cdot \widehat{\overrightarrow{u}h} + \hat{h}'NetLW' + \hat{h}'NetSW' + \hat{h}'SEF', \tag{3}$$

where primes denote anomalies relative to the spatial mean and hats denote the mass-weighted column integral. $\hat{h}'$ is the anomaly of vertically integrated FMSE, $\nabla_h \cdot \widehat{\overrightarrow{u}h}$ represents the horizontal transport, $NetLW'$ is the anomaly of column longwave convergence, $NetSW'$ is the anomaly of column shortwave convergence, and SEF' is the anomaly of surface enthalpy fluxes. Each term in eq. (3) is calculated for each grid column using hourly outputs. We calculate the horizontal convergence term, the first term on the right-hand side, as a residual from the rest of the terms in eq. (3) following previous studies that have done FMSE budget calculations (Bretherton et al., 2005; C. J. Muller & Held, 2012; Wing & Emanuel, 2014). We arrive at an equation for the spatial variance by normalizing each term by the instantaneous horizontal mean of $\hat{h}'^2$. We then average each term over the analysis period (day 100-120) over moist clusters and dry regions, respectively. The result of the calculation is demonstrated in Table 1.

The diabatic processes over moist clusters are more dominant in maintaining the aggregated state than they do over dry regions, as Table 1 shows that the terms over moist clusters are much greater than those over dry regions in both runs. Hence, we focus on the diabatic processes over moist clusters in the following analysis. We can see that advection and surface enthalpy fluxes are the terms that oppose aggregation, while the radiation terms support aggregation. The negative value of the advection term indicates that the deep circulation, which represents a positive gross moist stability (Neelin & Held, 1987), governs the advection term so that the overall large-scale circulation tends to stabilize moist clusters. The polluted run has a greater negative value of the advection term compared to that in the pristine run. As the aforementioned results have demonstrated that the polluted run has weaker deep circulation, we suspect that the greater negative value of the advection term results from the reduction in the upgradient energy transport by shallow circulation. The primary factor of the reduction appears to be the greater export of cloud water at mid-level in the polluted run, as cloud water is implicitly taken into account by FMSE.

The negative value of surface enthalpy fluxes term in both runs suggests that the negative air-sea enthalpy disequilibrium feedback (Wing & Emanuel, 2014) overcomes the positive wind-induced surface heat exchange (WISHE; K. A. Emanuel, 1987) feedback in our model. Because our simulations use a fixed, uniform SST, the air-sea enthalpy disequilibrium depends on the near-surface water vapor mixing ratio. In the polluted run, the less column moisture over moist clusters may be responsible for the less negative value of the surface enthalpy fluxes term compared to the pristine run. As for the radiation terms, pollution leads to a greater value of the longwave term and a lower value of the shortwave term, of which more cloud cover emitting less energy outward and less column moisture absorbing less energy may be the primary factor, respectively. Overall, the budget analysis demonstrates that the modulation of how the diabatic processes that support or oppose convective aggregation maintain the aggregated state at equilibrium is consistent with the other results in this study. To further quantify the cause and effect of a certain process associated with AIEs, a different experiment setup with a focus on the transition between equilibrium states is necessary but out of the scope of this study.

The current result demonstrates that pollution modulates the relative role of shallow circulation in the overall energy transport under the equilibrium state with weaker large-scale circulation. The enhancement in the mid-level cloud water export from moist clusters appears to be a key factor of the modulation. The aforementioned result implies that the enhancement may be related to the closeness of the convection to the moist cluster edges.

The heterogeneity of convection over space in moist clusters illustrated in Fig. 1 and Fig. 6 suggests that isolating deep convection from the environment is necessary to elucidate the difference in bulk attributes of convection features between the polluted and the pristine run. We use the convective system identification method following Feng et al. (2019), defining cold cloud systems (CCSs) as contiguous grid cells with brightness temperature $T_b < 241\,K$. The OLR in our model outputs is converted to T_b following Yang and Slingo (2001). Fig.7 shows the mean vertical profiles of vertical velocity and hydrometeors mixing ratio within CCSs and the mean vertical profile of cloud water mixing ratio over regions in moist clusters but not defined as a CCS. We can see that the CCSs have top-heavy vertical profiles in both runs, while the polluted run has weaker mean vertical velocity (Fig. 7a). The weaker vertical velocities in the polluted run imply smaller condensation and deposition rates and lesser buoyancy production aloft. Consistent with this idea, there is less cloud ice within the polluted run (Fig. 7b). On the other hand, the enhanced CCN concentration results in a larger fraction of liquid occurring as cloud water (rather than rain). The polluted run has a cloud water mixing ratio more than twice that of the pristine run over both the CCSs and the other regions in moist clusters (Fig. 7c-d). The higher cloud water mixing ratio over regions outside of CCSs in the polluted run compared to that in the pristine run implies that pollution may lead to an increase in mid-level static stability, which promotes detrainment of cloud water into the environment (Johnson et al., 1999; Posselt et al., 2008).

The warm rain amount in the polluted run is less than that in the pristine run (Fig. 7e), which is an expected result (Rosenfeld, 1999). The polluted run has more falling rimed ice at the mid-to-low level (400-850 hPa) and the near-surface (Fig. 7f), showing that the partition between cold rain and warm rain may be different between the two runs. However, the impact of pollution on the mixed-phase microphysical processes can not be isolated from the other controlling factors in our simulations because the two runs have contrasting environmental conditions.

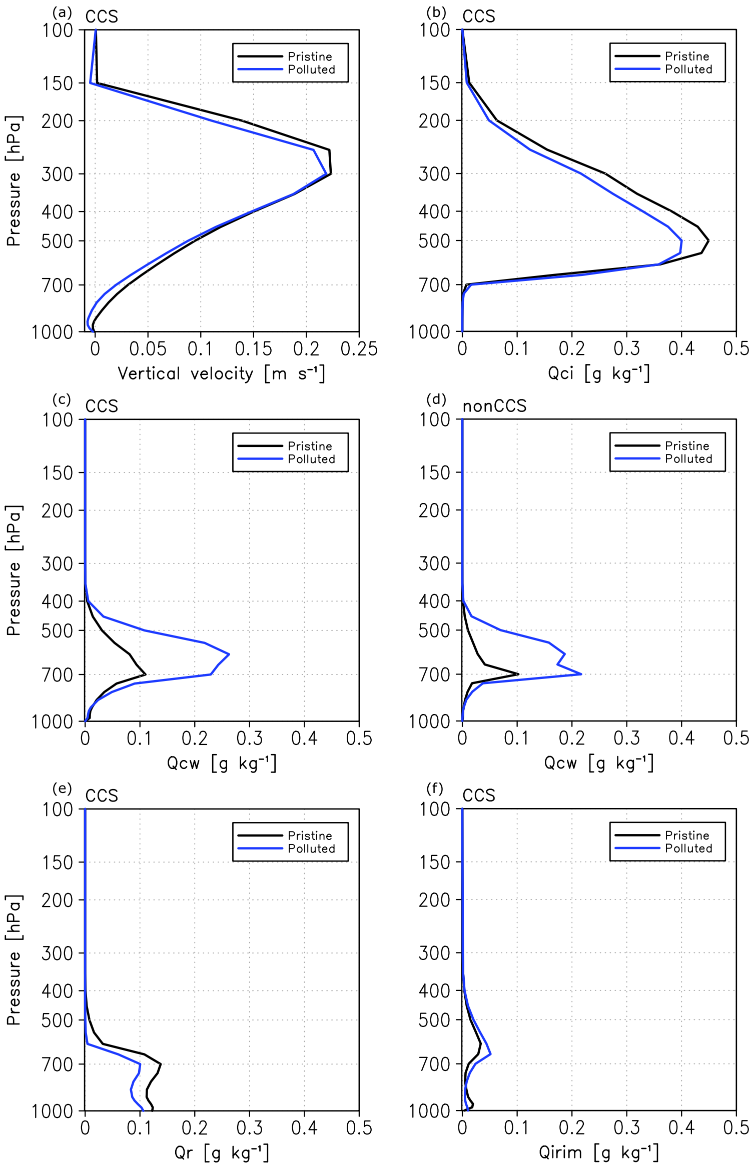

Figure 7. Vertical profiles of the mean vertical velocity and cloud ice, cloud water, rain water, and rimed cloud ice mixing ratio over the CCSs (a.b.c.e.f) and the mean profile of cloud water mixing ratio over the regions in moist clusters outside of CCSs (d).

A critical characteristic of tropical deep convection is the rapid intensification of precipitation once CWV has exceeded a critical value, which characterizes the effect of water vapor on the buoyancy of clouds through entrainment (Bretherton et al., 2004; Neelin et al., 2009; O. Peters & Neelin, 2006). We investigate the influence of pollution on this precipitation-CWV dependency. Analyses among all CCSs with a given CWV indicate that our simulations mimic the precipitation-CWV dependency seen in nature, with a rapid increase in precipitation (Fig. 8a) and updraft intensity (Fig. 8b-c) occurring above a certain threshold in CWV. However, a distinct difference between the polluted run and the pristine one is that the threshold CWV that heralds the increase in convective intensity occurs at a lower CWV value (53 mm) than it does in the pristine run (57 mm). On the other hand, the highest CWV environment over CCSs in the pristine run (>65 mm) is absent in the polluted run.

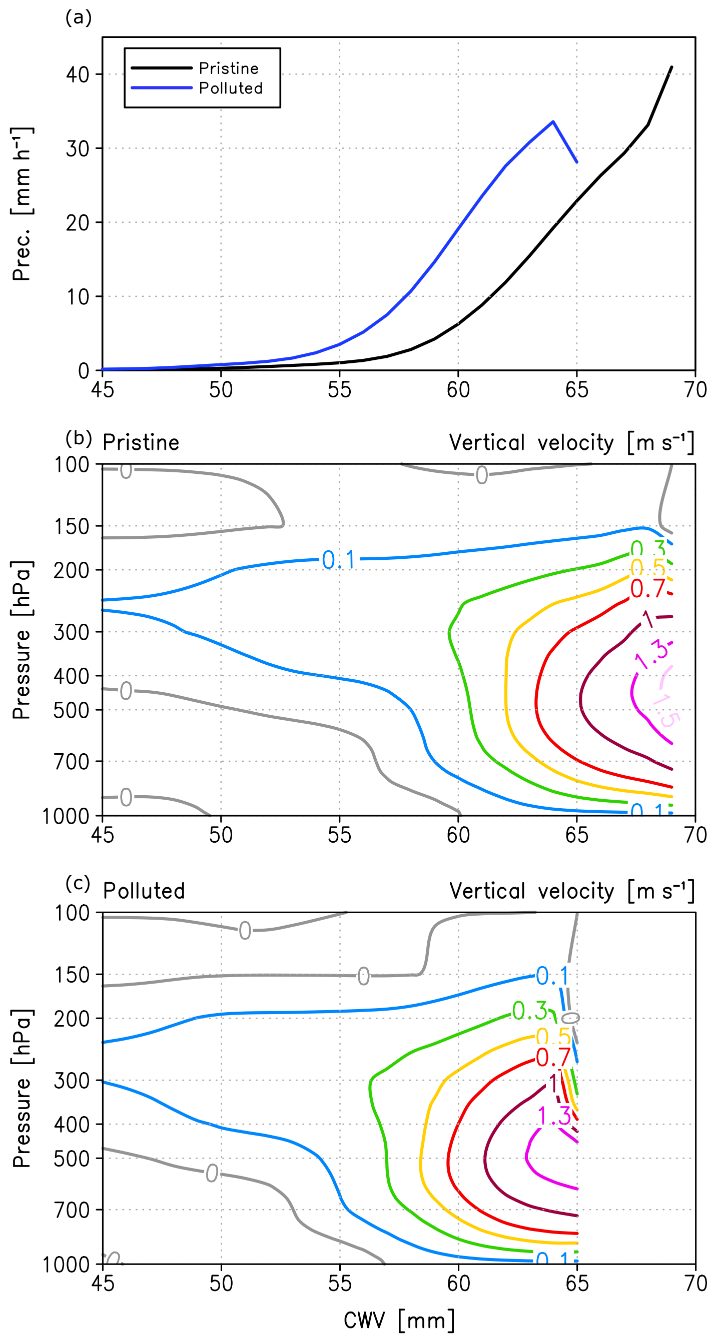

Figure 8. Precipitation intensity (a) and vertical velocity (b,c) within the CCSs conditional sampled by CWV from day 100 to 120.

Recall from Fig. 5a that mean CWV increases monotonically from dry regions toward moist clusters in both runs. We speculate that the spatial distribution of CCSs is a factor of the lower threshold CWV of rapid convection intensification in the polluted run. We apply the tracking analysis that links the CCSs overlapped in consecutive hourly outputs as a CCS track (Moseley et al., 2013) to find where CCSs start to develop. The tracked CCSs are classified into two categories according to how the CCS track initiates: emerging by itself and split from an existing CCS. Since our initiative is to identify the location where CCS triggering takes place, we only analyze the emerging tracks here.

Fig. 9 shows the distance-binned number of the emerging tracks with different present ages. The present age of a CCS is defined as the time difference between the present time step and the time step that the CCS emerged. In the polluted run, there are more tracks than the pristine run, and the maximum lifetime of the polluted tracks is longer. Tracks over dry regions have a shorter lifetime than tracks over moist clusters. The majority of young tracks (age<12 hr) in the polluted run are located at regions closer to the edge than they are in the pristine run. The result verifies our speculation that the CCSs in the polluted run start to develop at regions closer to the edge with a lower CWV at which strong near-surface convergence takes place.

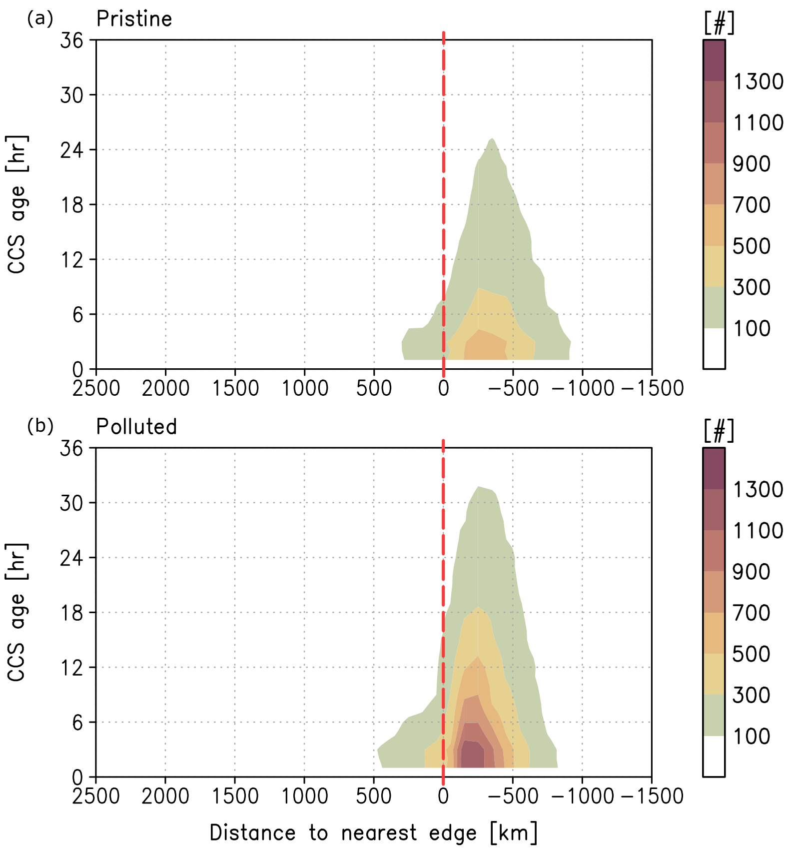

Figure 9. Number of CCSs with different present age (y-axis) conditionally sampled by the distance to the nearest edge in the pristine run (a) and the polluted run (b) from day 100 to 120.

Fig. 10a shows the probability distribution of the projected horizontal wind speed V_{in} at 1000 hPa over the regions of $0 < d < 50\,km$. Fig. 10b shows the probability distribution of the estimated cold pool propagation velocity (Rotunno et al., 1988) over the CCSs

$$V_{cp} = \sqrt{2 \int_0^H -g \frac{\theta_\rho - \overline{\theta_\rho}(k)}{\overline{\theta_\rho}(k)} \, dz}, \tag{4}$$

where θ_ρ is the density potential temperature (K. A. Emanuel, 1994), k is the index of the moist cluster, overbars denote the average in k moist cluster but outside of CCSs, and H is the height of the cold pool given by the height at which θ_ρ is no longer smaller than $\overline{\theta_\rho}(k)$. As expected, the polluted run has the weaker V_{in} at 1000 hPa over the regions close to the edge. On the other hand, the impact of pollution on the distribution of estimated cold pool velocity is subtle. The distribution is slightly wider in the parameter space in the polluted run. We note that the analyses here are column-based, whereas V_{in} and V_{cp} were calculated using the mean fields over the regions close to the edge of moist clusters in Windmiller and Hohenegger (2019). The difference in how the analysis is performed may influence the resulting V_{in} and V_{cp} individually. Our result highlights that the weakening of near-surface inflow corroborates the closeness of the convection to the moist cluster edges in the polluted run, although the distribution of V_{in} does not approximately match the distribution of V_{cp} as shown in Fig. 8a in Windmiller and Hohenegger (2019).

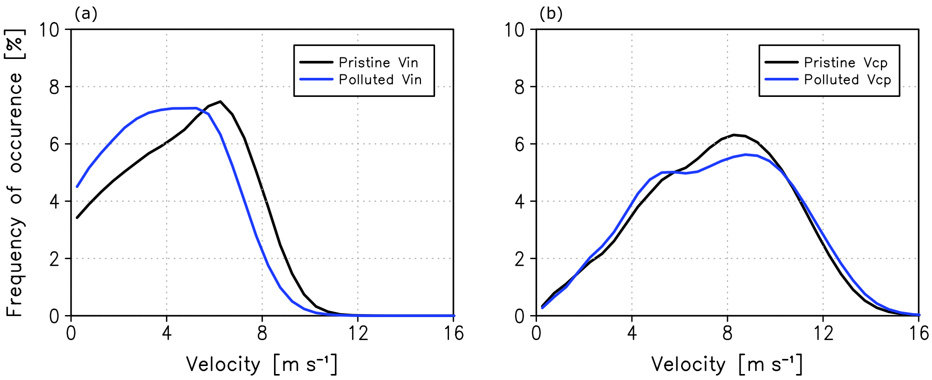

Figure 10. Probability distribution of V_{in} at 1000 hPa over the dry regions of $0 < d < 50\,km$ (a) and V_{cp} over the CCSs (b) from day 100 to 120.

Despite convection intensity starting to increase rapidly at a lower CWV in the polluted run, the two runs have the same increasing rate of convection intensity along with CWV. The CWV-binned precipitation intensities in the two runs can be collapsed by shifting the CWV by 4 mm. Why is the convection intensity limited in the polluted run (Fig. 7a)? We analyze the convective available potential energy (CAPE) for each moist cluster to identify the large-scale instability that constrains convection intensity. The CAPE is calculated as

$$CAPE_k = \int_{LFC}^{EL} B_k \, dz, \tag{5}$$

where k is the index of the moist cluster, LFC is the level of free convection, EL is the equilibrium level, and B_k is the buoyancy of the undiluted lifting parcel which is lifted adiabatically with freezing (J. M. Peters et al., 2022) from 2 m above ground level. The background environmental profile used for calculating B_k is the mean over regions within

k moist cluster but outside of CCSs. Fig. 11 shows the probability distribution of $CAPE$ of moist clusters larger than 500 km of horizontal scale. The result indicates that moist clusters in the polluted run generally have less large-scale instability. The suspected reduction in the upgradient energy transport by shallow circulation and the lower threshold CWV that may impede the accumulation of boundary layer moisture over moist clusters are both correlated to less CAPE in the polluted run. Overall, the polluted run has a weaker convection intensity compared to the pristine run.

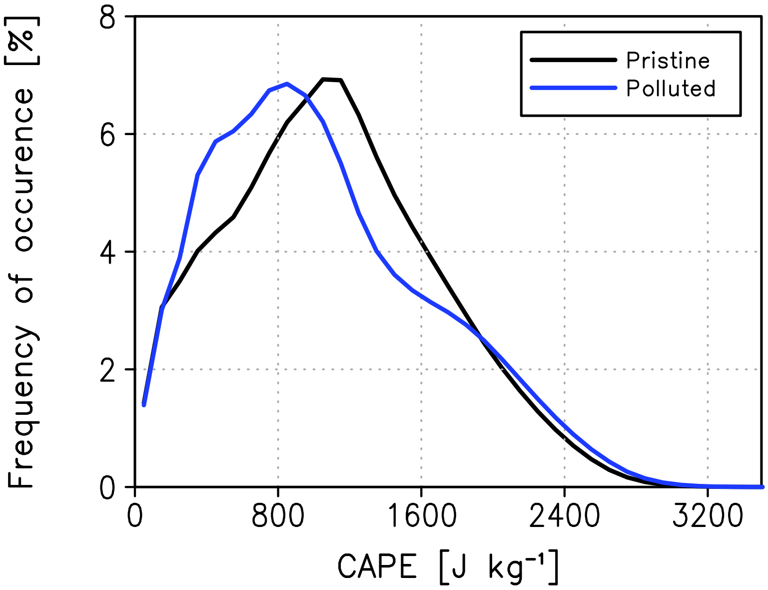

Figure 11. Moist cluster-based probability distribution of CAPE from day 100 to 120.

4 Summary and Discussion

This study investigates the modulation of tropical convection-circulation interaction by enhanced CCN concentrations using a pair of non-rotating RCE simulations with the uniform and fixed SST of 300K of a global convection-permitting model. The model explicitly simulates the dynamic response of deep convection to the enhanced CCN concentration and allows deep convection to interact with large-scale circulation without artificial constraints of scale separation assumption and the geometry of the simulation domain. The idealized setup of constant background aerosol concentration in the two simulations, namely the pristine run and the polluted run, is used to examine the changes in convection variability over space and the pattern of large-scale circulation with pollution. We analyze the difference between the pristine run and the polluted run at a statistical equilibrium state of RCE in which the convective self-aggregation processes had occurred, resulting in an aggregated state maintained by large-scale circulations.

We found that pollution weakens large-scale circulations, including the deep circulation and the shallow circulation, and leads to a mean state with a lower degree of convective aggregation. Analysis of cold cloud systems tracking shows that deep convective systems in the polluted run have notably more mid-level cloud water compared to the pristine run, and they preferably start to develop over regions close to the edge of moist clusters, contributing to the export of cloud water from moist clusters to dry regions. Pollution modulates how the diabatic processes that support or oppose convective aggregation maintain the aggregated state at equilibrium, including the role of shallow circulation in the energy transport between moist clusters and dry regions. Overall, the analysis of precipitation-CWV dependency suggests that pollution facilitates the development of deep convection in a drier environment but reduces the large-scale instability and the convection intensity. Our results emphasize the importance of allowing atmospheric phenomena to evolve continuously across spatial and temporal scales in simulations when investigating the response of tropical convection to changes in cloud microphysics. To our knowledge, this is the first study that simultaneously simulates the response of deep convection to changes in cloud microphysics and postulates the impact of pollution on the interaction between system-based tropical convection features and large-scale circulation that develops without the limitation of horizontal scale.

Similarities between our results and previous studies of aerosol indirect effects on tropical troposphere include weakened convection intensity (Beydoun & Hoose, 2019; Morrison & Grabowski, 2011), atmospheric cooling (Nishant et al., 2019; Dagan, 2022), and weakened convective aggregation (Beydoun & Hoose, 2019). However, there are contrasting physical processes leading to the results. For example, enhanced high clouds amount due to pollution leading to weaker tropospheric destabilization through radiative effects are found critical to weakening convection in Morrison and Grabowski (2011) and Beydoun and Hoose (2019). The polluted run has a less high cloud amount compared to the pristine run in this study (Fig. 4 and Fig. 7). We suspect that the contrasting result in the dependence of high clouds amount to pollution may be model dependent since the representation of mixed-phase microphysical processes is believed to drive the large difference in tropical high clouds among the GCPMs (Nugent et al., 2022; Roh et al., 2021; Turbeville et al., 2022). The equilibrium state analysis here provides a reference for studies aiming at finding causal relationships between physical processes. An investigation focusing on the transition phase between different aggregated states due to pollution will be carried out by the co-authors.

The current model runs at the horizontal resolution of around 15 km so that the minimum scale of deep convection development is close to the scale of convective updraft cores within an organized convective system (Houze, 2018). While we focus on the changes in the multi-scale coupling processes associated with the response of tropical deep convection to pollution, the study of van den Heever et al. (2011) suggested that aerosol indirect effects associated with tropical shallow clouds may offset or compensate for the aerosol indirect effects associated with congestus and deep convection systems and vice versa. We expect studies with the inclusion of the response of shallow convection to pollution using the current research framework to come in the future. Parallel modeling efforts to further depict the natural variability include heterogeneous aerosol perturbations, cloud-aerosol interactions, air-sea interactions, and aerosol direct radiative effects.

A possible real-world manifestation of our result is the convection activity over the Maritime Continent (MC) region. Past studies indicated that the large-scale organization of convection in non-rotating RCE simulations and MJO-like (i.e., Madden-Julian Oscillation; Madden & Julian, 1971) disturbance in rotating RCE simulations share the same driving mechanism (i.e., cloud-radiation feedbacks) in which AIEs can be critical (Arnold & Randall, 2015; Khairoutdinov & Emanuel, 2018). One of the leading theories of MJO propagation is that MJOs suffer from a barrier effect when they propagate over the MC (Kim et al., 2014; Zhang & Ling, 2017). The development of convective systems over the ocean in the MC plays a crucial role in carrying the MJO signal (Ling et al., 2019). As the MC is a major source of different types of aerosol around the globe (Reid et al., 2012; Salinas et al., 2013; Shpund et al., 2019), evaluation of sub-seasonal hindcasts spanning an active MJO event can be carried out to investigate the observed relationship between the geographical distribution of convective systems and aerosol emission scenarios.

5 Open Research

A temporal snapshot of CWV, grid column distance to the nearest moist cluster edge, CCS, and the GrADS plotting scripts are available at https://doi.org/10.6084/m9.figshare.22149617.v2.

Acknowledgments

Chun-Yian Su and J. Peter's efforts were supported by National Science Foundation (NSF) grants AGS-1928666, AGS-1841674, and the Department of Energy Atmospheric System Research (DOE ASR) grant DE-SC0000246356. Chien-Ming Wu and Chun-Yian Su's efforts were supported by National Science and Technology Council of Taiwan grant 111-2111-M-002-012-NSTC. Wei-Ting Chen was supported by National Science and Technology Council of Taiwan grants NSTC112-2111-M-002-008, NSTC112-2111-M-002-015, and National Taiwan University grants NTU-112L7832 and NTU-112L7858. We thank Dr. Jen-Her Chen in Central Weather Bureau for his support of this work.

References

Abbott, T. H., & Cronin, T. W. (2021, January). Aerosol invigoration of atmospheric convection through increases in humidity. *Science*, *371*(6524), 83–85. Retrieved from `https://doi.org/10.1126/science.abc5181` doi: 10.1126/science.abc5181

Anber, U. M., Wang, S., Gentine, P., & Jensen, M. P. (2019, September). Probing the response of tropical deep convection to aerosol perturbations using idealized cloud-resolving simulations with parameterized large-scale dynamics. *Journal of the Atmospheric Sciences*, *76*(9), 2885–2897. Retrieved from `https://doi.org/10.1175/jas-d-18-0351.1` doi: 10.1175/jas-d-18-0351.1

Andreae, M. O. (2009, January). Correlation between cloud condensation nuclei concentration and aerosol optical thickness in remote and polluted regions. *Atmospheric Chemistry and Physics*, *9*(2), 543–556. Retrieved from `https://doi.org/10.5194/acp-9-543-2009` doi: 10.5194/acp-9-543-2009

Andreae, M. O., Rosenfeld, D., Artaxo, P., Costa, A. A., Frank, G. P., Longo, K. M., & Silva-Dias, M. A. F. (2004, February). Smoking rain clouds over the amazon. *Science*, *303*(5662), 1337–1342. Retrieved from `https://doi.org/10.1126/science.1092779` doi: 10.1126/science.1092779

Arakawa, A. (2004, July). The cumulus parameterization problem: Past, present, and future. *Journal of Climate*, *17*(13), 2493–2525. Retrieved from `https://doi.org/10.1175/1520-0442(2004)017<2493:ratcpp>2.0.co;2` doi: 10.1175/1520-0442(2004)017⟨2493:ratcpp⟩2.0.co;2

Arakawa, A., & Wu, C.-M. (2013, July). A unified representation of deep moist convection in numerical modeling of the atmosphere. part i. *Journal of the Atmospheric Sciences*, *70*(7), 1977–1992. Retrieved from `https://doi.org/10.1175/jas-d-12-0330.1` doi: 10.1175/jas-d-12-0330.1

Arnold, N. P., & Putman, W. M. (2018, April). Nonrotating convective self-aggregation in a limited area AGCM. *Journal of Advances in Modeling Earth Systems*, *10*(4), 1029–1046. Retrieved from `https://doi.org/10.1002/2017ms001218` doi: 10.1002/2017ms001218

Arnold, N. P., & Randall, D. A. (2015, October). Global-scale convective aggregation: Implications for the madden-julian oscillation. *Journal of Advances in Modeling Earth Systems*, *7*(4), 1499–1518. Retrieved from `https://doi.org/10.1002/2015ms000498` doi: 10.1002/2015ms000498

Becker, T., Bretherton, C. S., Hohenegger, C., & Stevens, B. (2018, January). Estimating bulk entrainment with unaggregated and aggregated convection. *Geophysical Research Letters*, *45*(1), 455–462. Retrieved from `https://doi.org/10.1002/2017gl076640` doi: 10.1002/2017gl076640

Beydoun, H., & Hoose, C. (2019, April). Aerosol-cloud-precipitation interactions in the context of convective self-aggregation. *Journal of Advances in Modeling Earth Systems*, *11*(4), 1066–1087. Retrieved from https://doi.org/10.1029/2018ms001523 doi: 10.1029/2018ms001523

Bretherton, C. S., Blossey, P. N., & Khairoutdinov, M. (2005, December). An energy-balance analysis of deep convective self-aggregation above uniform SST. *Journal of the Atmospheric Sciences*, *62*(12), 4273–4292. Retrieved from https://doi.org/10.1175/jas3614.1 doi: 10.1175/jas3614.1

Bretherton, C. S., Peters, M. E., & Back, L. E. (2004, April). Relationships between water vapor path and precipitation over the tropical oceans. *Journal of Climate*, *17*(7), 1517–1528. Retrieved from https://doi.org/10.1175/1520-0442(2004)017<1517:rbwvpa>2.0.co;2 doi: 10.1175/1520-0442(2004)017⟨1517:rbwvpa⟩2.0.co;2

Caldwell, P. M., Terai, C. R., Hillman, B., Keen, N. D., Bogenschutz, P., Lin, W., … Zender, C. S. (2021, November). Convection-permitting simulations with the e3sm global atmosphere model. *Journal of Advances in Modeling Earth Systems*, *13*(11). Retrieved from https://doi.org/10.1029/2021ms002544 doi: 10.1029/2021ms002544

Chang, Y.-H., Chen, W.-T., Wu, C.-M., Moseley, C., & Wu, C.-C. (2021, November). Tracking the influence of cloud condensation nuclei on summer diurnal precipitating systems over complex topography in taiwan. *Atmospheric Chemistry and Physics*, *21*(22), 16709–16725. Retrieved from https://doi.org/10.5194/acp-21-16709-2021 doi: 10.5194/acp-21-16709-2021

Coppin, D., & Bony, S. (2015, December). Physical mechanisms controlling the initiation of convective self-aggregation in a general circulation model. *Journal of Advances in Modeling Earth Systems*, *7*(4), 2060–2078. Retrieved from https://doi.org/10.1002/2015ms000571 doi: 10.1002/2015ms000571

Cronin, T. W., & Wing, A. A. (2017, December). Clouds, circulation, and climate sensitivity in a radiative-convective equilibrium channel model. *Journal of Advances in Modeling Earth Systems*, *9*(8), 2883–2905. Retrieved from https://doi.org/10.1002/2017ms001111 doi: 10.1002/2017ms001111

Dagan, G. (2022, December). Equilibrium climate sensitivity increases with aerosol concentration due to changes in precipitation efficiency. *Atmospheric Chemistry and Physics*, *22*(24), 15767–15775. Retrieved from https://doi.org/10.5194/acp-22-15767-2022 doi: 10.5194/acp-22-15767-2022

Dunion, J. P. (2011, February). Rewriting the climatology of the tropical north atlantic and caribbean sea atmosphere. *Journal of Climate*, *24*(3), 893–908. Retrieved from https://doi.org/10.1175/2010jcli3496.1 doi: 10.1175/2010jcli3496.1

Emanuel, K., Wing, A. A., & Vincent, E. M. (2014, February). Radiative-convective instability. *Journal of Advances in Modeling Earth Systems*, *6*(1), 75–90. Retrieved from https://doi.org/10.1002/2013ms000270 doi: 10.1002/2013ms000270

Emanuel, K. A. (1987, August). An air-sea interaction model of intraseasonal oscillations in the tropics. *Journal of the Atmospheric Sciences*, *44*(16), 2324–2340. Retrieved from https://doi.org/10.1175/1520-0469(1987)044<2324:aasimo>2.0.co;2 doi: 10.1175/1520-0469(1987)044⟨2324:aasimo⟩2.0.co;2

Emanuel, K. A. (1994). *Atmospheric convection*. Oxford University Press, USA.

Fan, J., & Khain, A. (2021, January). Comments on "do ultrafine cloud condensation nuclei invigorate deep convection?". *Journal of the Atmospheric Sciences*, *78*(1), 329–339. Retrieved from https://doi.org/10.1175/jas-d-20-0218.1 doi: 10.1175/jas-d-20-0218.1

Fan, J., Rosenfeld, D., Zhang, Y., Giangrande, S. E., Li, Z., Machado, L. A. T., … de Souza, R. A. F. (2018, January). Substantial convection and precipitation enhancements by ultrafineaerosol particles. *Science*, *359*(6374), 411–418. Retrieved from https://doi.org/10.1126/science.aan8461 doi:

10.1126/science.aan8461

Fan, J., Wang, Y., Rosenfeld, D., & Liu, X. (2016, October). Review of aerosol–cloud interactions: Mechanisms, significance, and challenges. *Journal of the Atmospheric Sciences*, *73*(11), 4221–4252. Retrieved from `https://doi.org/10.1175/jas-d-16-0037.1` doi: 10.1175/jas-d-16-0037.1

Fan, J., Yuan, T., Comstock, J. M., Ghan, S., Khain, A., Leung, L. R., … Ovchinnikov, M. (2009, November). Dominant role by vertical wind shear in regulating aerosol effects on deep convective clouds. *Journal of Geophysical Research*, *114*(D22). Retrieved from `https://doi.org/10.1029/2009jd012352` doi: 10.1029/2009jd012352

Feng, Z., Houze, R. A., Leung, L. R., Song, F., Hardin, J. C., Wang, J., … Homeyer, C. R. (2019, September). Spatiotemporal characteristics and large-scale environments of mesoscale convective systems east of the rocky mountains. *Journal of Climate*, *32*(21), 7303–7328. Retrieved from `https://doi.org/10.1175/jcli-d-19-0137.1` doi: 10.1175/jcli-d-19-0137.1

Feng, Z., Leung, L. R., Hardin, J., Terai, C. R., Song, F., & Caldwell, P. (2023, February). Mesoscale convective systems in DYAMOND global convection-permitting simulations. *Geophysical Research Letters*, *50*(4). Retrieved from `https://doi.org/10.1029/2022gl102603` doi: 10.1029/2022gl102603

Grabowski, W. W. (2018, October). Can the impact of aerosols on deep convection be isolated from meteorological effects in atmospheric observations? *Journal of the Atmospheric Sciences*, *75*(10), 3347–3363. Retrieved from `https://doi.org/10.1175/jas-d-18-0105.1` doi: 10.1175/jas-d-18-0105.1

Grabowski, W. W., & Morrison, H. (2020, July). Do ultrafine cloud condensation nuclei invigorate deep convection? *Journal of the Atmospheric Sciences*, *77*(7), 2567–2583. Retrieved from `https://doi.org/10.1175/jas-d-20-0012.1` doi: 10.1175/jas-d-20-0012.1

Grabowski, W. W., & Morrison, H. (2021, January). Reply to "comments on 'do ultrafine cloud condensation nuclei invigorate deep convection?'". *Journal of the Atmospheric Sciences*, *78*(1), 341–350. Retrieved from `https://doi.org/10.1175/jas-d-20-0315.1` doi: 10.1175/jas-d-20-0315.1

Hartmann, D. L., Moy, L. A., & Fu, Q. (2001, December). Tropical convection and the energy balance at the top of the atmosphere. *Journal of Climate*, *14*(24), 4495–4511. Retrieved from `https://doi.org/10.1175/1520-0442(2001)014<4495:tcateb>2.0.co;2` doi: 10.1175/1520-0442(2001)014⟨4495:tcateb⟩2.0.co;2

Hohenegger, C., Korn, P., Linardakis, L., Redler, R., Schnur, R., Adamidis, P., … Stevens, B. (2023, January). ICON-sapphire: simulating the components of the earth system and their interactions at kilometer and subkilometer scales. *Geoscientific Model Development*, *16*(2), 779–811. Retrieved from `https://doi.org/10.5194/gmd-16-779-2023` doi: 10.5194/gmd-16-779-2023

Holloway, C. E., & Woolnough, S. J. (2016, February). The sensitivity of convective aggregation to diabatic processes in idealized radiative-convective equilibrium simulations. *Journal of Advances in Modeling Earth Systems*, *8*(1), 166–195. Retrieved from `https://doi.org/10.1002/2015ms000511` doi: 10.1002/2015ms000511

Houze, R. A. (2004, December). Mesoscale convective systems. *Reviews of Geophysics*, *42*(4). Retrieved from `https://doi.org/10.1029/2004rg000150` doi: 10.1029/2004rg000150

Houze, R. A. (2018, January). 100 years of research on mesoscale convective systems. *Meteorological Monographs*, *59*, 17.1–17.54. Retrieved from `https://doi.org/10.1175/amsmonographs-d-18-0001.1` doi: 10.1175/amsmonographs-d-18-0001.1

Igel, A. L., & van den Heever, S. C. (2021, August). Invigoration or enervation of convective clouds by aerosols? *Geophysical Research Letters*, *48*(16). Retrieved from https://doi.org/10.1029/2021gl093804 doi: 10.1029/2021gl093804

Jeevanjee, N., & Romps, D. M. (2013, March). Convective self-aggregation, cold pools, and domain size. *Geophysical Research Letters*, *40*(5), 994–998. Retrieved from https://doi.org/10.1002/grl.50204 doi: 10.1002/grl.50204

Johnson, R. H., Rickenbach, T. M., Rutledge, S. A., Ciesielski, P. E., & Schubert, W. H. (1999, August). Trimodal characteristics of tropical convection. *Journal of Climate*, *12*(8), 2397–2418. Retrieved from https://doi.org/10.1175/1520-0442(1999)012<2397:tcotc>2.0.co;2 doi: 10.1175/1520-0442(1999)012⟨2397:tcotc⟩2.0.co;2

Khain, A. P., BenMoshe, N., & Pokrovsky, A. (2008, June). Factors determining the impact of aerosols on surface precipitation from clouds: An attempt at classification. *Journal of the Atmospheric Sciences*, *65*(6), 1721–1748. Retrieved from https://doi.org/10.1175/2007jas2515.1 doi: 10.1175/2007jas2515.1

Khairoutdinov, M. F., & Emanuel, K. (2018, December). Intraseasonal variability in a cloud-permitting near-global equatorial aquaplanet model. *Journal of the Atmospheric Sciences*, *75*(12), 4337–4355. Retrieved from https://doi.org/10.1175/jas-d-18-0152.1 doi: 10.1175/jas-d-18-0152.1

Kiladis, G. N., Wheeler, M. C., Haertel, P. T., Straub, K. H., & Roundy, P. E. (2009, April). Convectively coupled equatorial waves. *Reviews of Geophysics*, *47*(2). Retrieved from https://doi.org/10.1029/2008rg000266 doi: 10.1029/2008rg000266

Kim, D., Kug, J.-S., & Sobel, A. H. (2014, January). Propagating versus non-propagating madden–julian oscillation events. *Journal of Climate*, *27*(1), 111–125. Retrieved from https://doi.org/10.1175/jcli-d-13-00084.1 doi: 10.1175/jcli-d-13-00084.1

Koren, I., Feingold, G., & Remer, L. A. (2010, September). The invigoration of deep convective clouds over the atlantic: aerosol effect, meteorology or retrieval artifact? *Atmospheric Chemistry and Physics*, *10*(18), 8855–8872. Retrieved from https://doi.org/10.5194/acp-10-8855-2010 doi: 10.5194/acp-10-8855-2010

Koren, I., Martins, J. V., Remer, L. A., & Afargan, H. (2008, August). Smoke invigoration versus inhibition of clouds over the amazon. *Science*, *321*(5891), 946–949. Retrieved from https://doi.org/10.1126/science.1159185 doi: 10.1126/science.1159185

Lau, K.-H., & Lau, N.-C. (1990, September). Observed structure and propagation characteristics of tropical summertime synoptic scale disturbances. *Monthly Weather Review*, *118*(9), 1888–1913. Retrieved from https://doi.org/10.1175/1520-0493(1990)118<1888:osapco>2.0.co;2 doi: 10.1175/1520-0493(1990)118⟨1888:osapco⟩2.0.co;2

Lebo, Z. (2018, February). A numerical investigation of the potential effects of aerosol-induced warming and updraft width and slope on updraft intensity in deep convective clouds. *Journal of the Atmospheric Sciences*, *75*(2), 535–554. Retrieved from https://doi.org/10.1175/jas-d-16-0368.1 doi: 10.1175/jas-d-16-0368.1

Ling, J., Zhang, C., Joyce, R., ping Xie, P., & Chen, G. (2019, March). Possible role of the diurnal cycle in land convection in the barrier effect on the MJO by the maritime continent. *Geophysical Research Letters*, *46*(5), 3001–3011. Retrieved from https://doi.org/10.1029/2019gl081962 doi: 10.1029/2019gl081962

Madden, R. A., & Julian, P. R. (1971, July). Detection of a 40–50 day oscillation in the zonal wind in the tropical pacific. *Journal of the Atmospheric Sciences*, *28*(5), 702–708. Retrieved from https://doi.org/10.1175/1520-0469(1971)028<0702:doadoi>2.0.co;2 doi: 10.1175/1520-0469(1971)028⟨0702:doadoi⟩2.0.co;2

Manabe, S., & Strickler, R. F. (1964, July). Thermal equilibrium of the atmosphere with a convective adjustment. *Journal of the Atmospheric Sciences*, *21*(4), 361–385. Retrieved from https://doi.org/10.1175/1520-0469(1964)021<0361:teotaw>2.0.co;2 doi: 10.1175/1520-0469(1964)021⟨0361:teotaw⟩2.0.co;2

Mapes, B. E., Chung, E. S., Hannah, W. M., Masunaga, H., Wimmers, A. J., & Velden, C. S. (2018, January). The meandering margin of the meteorological moist tropics. *Geophysical Research Letters*, *45*(2), 1177–1184. Retrieved from https://doi.org/10.1002/2017gl076440 doi: 10.1002/2017gl076440

Matsugishi, S., & Satoh, M. (2022, May). Sensitivity of the horizontal scale of convective self-aggregation to sea surface temperature in radiative convective equilibrium experiments using a global nonhydrostatic model. *Journal of Advances in Modeling Earth Systems*, *14*(5). Retrieved from https://doi.org/10.1029/2021ms002636 doi: 10.1029/2021ms002636

Morrison, H., & Grabowski, W. W. (2007, August). Comparison of bulk and bin warm-rain microphysics models using a kinematic framework. *Journal of the Atmospheric Sciences*, *64*(8), 2839–2861. Retrieved from https://doi.org/10.1175/jas3980 doi: 10.1175/jas3980

Morrison, H., & Grabowski, W. W. (2008, March). Modeling supersaturation and subgrid-scale mixing with two-moment bulk warm microphysics. *Journal of the Atmospheric Sciences*, *65*(3), 792–812. Retrieved from https://doi.org/10.1175/2007jas2374.1 doi: 10.1175/2007jas2374.1

Morrison, H., & Grabowski, W. W. (2011, October). Cloud-system resolving model simulations of aerosol indirect effects on tropical deep convection and its thermodynamic environment. *Atmospheric Chemistry and Physics*, *11*(20), 10503–10523. Retrieved from https://doi.org/10.5194/acp-11-10503-2011 doi: 10.5194/acp-11-10503-2011

Morrison, H., & Milbrandt, J. A. (2015, January). Parameterization of cloud microphysics based on the prediction of bulk ice particle properties. part i: Scheme description and idealized tests. *Journal of the Atmospheric Sciences*, *72*(1), 287–311. Retrieved from https://doi.org/10.1175/jas-d-14-0065.1 doi: 10.1175/jas-d-14-0065.1

Moseley, C., Berg, P., & Haerter, J. O. (2013, dec). Probing the precipitation life cycle by iterative rain cell tracking. *Journal of Geophysical Research: Atmospheres*, *118*(24), 13,361–13,370. Retrieved from https://doi.org/10.1002%2F2013jd020868 doi: 10.1002/2013jd020868

Muller, C., Yang, D., Craig, G., Cronin, T., Fildier, B., Haerter, J. O., … Sherwood, S. C. (2022, January). Spontaneous aggregation of convective storms. *Annual Review of Fluid Mechanics*, *54*(1), 133–157. Retrieved from https://doi.org/10.1146/annurev-fluid-022421-011319 doi: 10.1146/annurev-fluid-022421-011319

Muller, C. J., & Held, I. M. (2012, August). Detailed investigation of the self-aggregation of convection in cloud-resolving simulations. *Journal of the Atmospheric Sciences*, *69*(8), 2551–2565. Retrieved from https://doi.org/10.1175/jas-d-11-0257.1 doi: 10.1175/jas-d-11-0257.1

Neelin, J. D., & Held, I. M. (1987, January). Modeling tropical convergence based on the moist static energy budget. *Monthly Weather Review*, *115*(1), 3–12. Retrieved from https://doi.org/10.1175/1520-0493(1987)115<0003:mtcbot>2.0.co;2 doi: 10.1175/1520-0493(1987)115⟨0003:mtcbot⟩2.0.co;2

Neelin, J. D., Peters, O., & Hales, K. (2009, August). The transition to strong convection. *Journal of the Atmospheric Sciences*, *66*(8), 2367–2384. Retrieved from https://doi.org/10.1175/2009jas2962.1 doi: 10.1175/2009jas2962.1

Nishant, N., & Sherwood, S. C. (2017, June). A cloud-resolving model study of aerosol-cloud correlation in a pristine maritime environment. *Geophysical Research Letters*, *44*(11), 5774–5781. Retrieved from https://doi.org/10.1002/2017gl073267 doi: 10.1002/2017gl073267

Nishant, N., Sherwood, S. C., & Geoffroy, O. (2019, September). Aerosol-induced modification of organised convection and top-of-atmosphere radiation. *npj Climate and Atmospheric Science*, *2*(1). Retrieved from `https://doi.org/10.1038/s41612-019-0089-1` doi: 10.1038/s41612-019-0089-1

Niu, F., & Li, Z. (2012, September). Systematic variations of cloud top temperature and precipitation rate with aerosols over the global tropics. *Atmospheric Chemistry and Physics*, *12*(18), 8491–8498. Retrieved from `https://doi.org/10.5194/acp-12-8491-2012` doi: 10.5194/acp-12-8491-2012

Nugent, J. M., Turbeville, S. M., Bretherton, C. S., Blossey, P. N., & Ackerman, T. P. (2022, February). Tropical cirrus in global storm-resolving models: 1. role of deep convection. *Earth and Space Science*, *9*(2). Retrieved from `https://doi.org/10.1029/2021ea001965` doi: 10.1029/2021ea001965

Pan, Z., Rosenfeld, D., Zhu, Y., Mao, F., Gong, W., Zang, L., & Lu, X. (2021, May). Observational quantification of aerosol invigoration for deep convective cloud lifecycle properties based on geostationary satellite. *Journal of Geophysical Research: Atmospheres*, *126*(9). Retrieved from `https://doi.org/10.1029/2020jd034275` doi: 10.1029/2020jd034275

Patrizio, C. R., & Randall, D. A. (2019, July). Sensitivity of convective self-aggregation to domain size. *Journal of Advances in Modeling Earth Systems*, *11*(7), 1995–2019. Retrieved from `https://doi.org/10.1029/2019ms001672` doi: 10.1029/2019ms001672

Pendergrass, A. G., Reed, K. A., & Medeiros, B. (2016, November). The link between extreme precipitation and convective organization in a warming climate: Global radiative-convective equilibrium simulations. *Geophysical Research Letters*, *43*(21). Retrieved from `https://doi.org/10.1002/2016gl071285` doi: 10.1002/2016gl071285

Peters, J. M., Lebo, Z. J., Chavas, D. R., & Su, C.-Y. (2023, June). Entrainment makes pollution more likely to weaken deep convective updrafts than invigorate them. *Geophysical Research Letters*, *50*(12). Retrieved from `https://doi.org/10.1029/2023gl103314` doi: 10.1029/2023gl103314

Peters, J. M., Mulholland, J. P., & Chavas, D. R. (2022, March). Generalized lapse rate formulas for use in entraining CAPE calculations. *Journal of the Atmospheric Sciences*, *79*(3), 815–836. Retrieved from `https://doi.org/10.1175/jas-d-21-0118.1` doi: 10.1175/jas-d-21-0118.1

Peters, O., & Neelin, J. D. (2006, May). Critical phenomena in atmospheric precipitation. *Nature Physics*, *2*(6), 393–396. Retrieved from `https://doi.org/10.1038/nphys314` doi: 10.1038/nphys314

Popke, D., Stevens, B., & Voigt, A. (2013, January). Climate and climate change in a radiative-convective equilibrium version of ECHAM6. *Journal of Advances in Modeling Earth Systems*, *5*(1), 1–14. Retrieved from `https://doi.org/10.1029/2012ms000191` doi: 10.1029/2012ms000191

Posselt, D. J., van den Heever, S. C., & Stephens, G. L. (2008, April). Trimodal cloudiness and tropical stable layers in simulations of radiative convective equilibrium. *Geophysical Research Letters*, *35*(8). Retrieved from `https://doi.org/10.1029/2007gl033029` doi: 10.1029/2007gl033029

Reid, J. S., Xian, P., Hyer, E. J., Flatau, M. K., Ramirez, E. M., Turk, F. J., … Maloney, E. D. (2012, February). Multi-scale meteorological conceptual analysis of observed active fire hotspot activity and smoke optical depth in the maritime continent. *Atmospheric Chemistry and Physics*, *12*(4), 2117–2147. Retrieved from `https://doi.org/10.5194/acp-12-2117-2012` doi: 10.5194/acp-12-2117-2012

Roh, W., Satoh, M., & Hohenegger, C. (2021). Intercomparison of cloud properties in DYAMOND simulations over the atlantic ocean. *Journal of the Meteorological Society of Japan. Ser. II*, *99*(6), 1439–1451. Retrieved from `https://doi.org/10.2151/jmsj.2021-070` doi: 10.2151/jmsj.2021-070

Romps, D. M., Latimer, K., Zhu, Q., Jurkat-Witschas, T., Mahnke, C., Prabhakaran, T., … Wendisch, M. (2023, January). Air pollution unable to intensify storms via warm-phase invigoration. *Geophysical Research Letters*, *50*(2). Retrieved from https://doi.org/10.1029/2022gl100409 doi: 10.1029/2022gl100409

Rosenfeld, D. (1999, October). TRMM observed first direct evidence of smoke from forest fires inhibiting rainfall. *Geophysical Research Letters*, *26*(20), 3105–3108. Retrieved from https://doi.org/10.1029/1999gl006066 doi: 10.1029/1999gl006066

Rosenfeld, D., Lohmann, U., Raga, G. B., O'Dowd, C. D., Kulmala, M., Fuzzi, S., … Andreae, M. O. (2008, September). Flood or drought: How do aerosols affect precipitation? *Science*, *321*(5894), 1309–1313. Retrieved from https://doi.org/10.1126/science.1160606 doi: 10.1126/science.1160606

Rotunno, R., Klemp, J. B., & Weisman, M. L. (1988, February). A theory for strong, long-lived squall lines. *Journal of the Atmospheric Sciences*, *45*(3), 463–485. Retrieved from https://doi.org/10.1175/1520-0469(1988)045<0463:atfsll>2.0.co;2 doi: 10.1175/1520-0469(1988)045⟨0463:atfsll⟩2.0.co;2

Salinas, S. V., Chew, B. N., Miettinen, J., Campbell, J. R., Welton, E. J., Reid, J. S., … Liew, S. C. (2013, March). Physical and optical characteristics of the october 2010 haze event over singapore: A photometric and lidar analysis. *Atmospheric Research*, *122*, 555–570. Retrieved from https://doi.org/10.1016/j.atmosres.2012.05.021 doi: 10.1016/j.atmosres.2012.05.021

Shpund, J., Khain, A., & Rosenfeld, D. (2019, August). Effects of sea spray on microphysics and intensity of deep convective clouds under strong winds. *Journal of Geophysical Research: Atmospheres*, *124*(16), 9484–9509. Retrieved from https://doi.org/10.1029/2018jd029893 doi: 10.1029/2018jd029893

Singh, M. S., & O'Gorman, P. A. (2013, August). Influence of entrainment on the thermal stratification in simulations of radiative-convective equilibrium. *Geophysical Research Letters*, *40*(16), 4398–4403. Retrieved from https://doi.org/10.1002/grl.50796 doi: 10.1002/grl.50796

Singh, M. S., & O'Gorman, P. A. (2015, June). Increases in moist-convective updraught velocities with warming in radiative-convective equilibrium. *Quarterly Journal of the Royal Meteorological Society*, *141*(692), 2828–2838. Retrieved from https://doi.org/10.1002/qj.2567 doi: 10.1002/qj.2567

Sobel, A. H., Nilsson, J., & Polvani, L. M. (2001, December). The weak temperature gradient approximation and balanced tropical moisture waves. *Journal of the Atmospheric Sciences*, *58*(23), 3650–3665. Retrieved from https://doi.org/10.1175/1520-0469(2001)058<3650:twtgaa>2.0.co;2 doi: 10.1175/1520-0469(2001)058⟨3650:twtgaa⟩2.0.co;2

Stevens, B., Satoh, M., Auger, L., Biercamp, J., Bretherton, C. S., Chen, X., … Zhou, L. (2019, September). DYAMOND: the DYnamics of the atmospheric general circulation modeled on non-hydrostatic domains. *Progress in Earth and Planetary Science*, *6*(1). Retrieved from https://doi.org/10.1186/s40645-019-0304-z doi: 10.1186/s40645-019-0304-z

Storer, R. L., & van den Heever, S. C. (2013, February). Microphysical processes evident in aerosol forcing of tropical deep convective clouds. *Journal of the Atmospheric Sciences*, *70*(2), 430–446. Retrieved from https://doi.org/10.1175/jas-d-12-076.1 doi: 10.1175/jas-d-12-076.1

Storer, R. L., van den Heever, S. C., & L'Ecuyer, T. S. (2014, April). Observations of aerosol-induced convective invigoration in the tropical east atlantic. *Journal of Geophysical Research: Atmospheres*, *119*(7), 3963–3975. Retrieved from https://doi.org/10.1002/2013jd020272 doi: 10.1002/2013jd020272

Su, C.-Y., Chen, W.-T., Wu, C.-M., & Ma, H.-Y. (2022). Object-based evaluation of tropical precipitation systems in DYAMOND simulations over the maritime continent. *Journal of the Meteorological Society of Japan. Ser. II*, *100*(4), 647–659. Retrieved from https://doi.org/10.2151/jmsj.2022-033 doi: 10.2151/jmsj.2022-033

Su, C.-Y., Wu, C.-M., Chen, W.-T., & Chen, J.-H. (2021a, July). The effects of the unified parameterization in the CWBGFS: the diurnal cycle of precipitation over land in the maritime continent. *Climate Dynamics*, *58*(1-2), 223–233. Retrieved from https://doi.org/10.1007/s00382-021-05899-2 doi: 10.1007/s00382-021-05899-2

Su, C.-Y., Wu, C.-M., Chen, W.-T., & Chen, J.-H. (2021b, October). Implementation of the unified representation of deep moist convection in the CWBGFS. *Monthly Weather Review*, *149*(10), 3525–3539. Retrieved from https://doi.org/10.1175/mwr-d-21-0067.1 doi: 10.1175/mwr-d-21-0067.1

Tao, W.-K., Chen, J.-P., Li, Z., Wang, C., & Zhang, C. (2012, April). Impact of aerosols on convective clouds and precipitation. *Reviews of Geophysics*, *50*(2). Retrieved from https://doi.org/10.1029/2011rg000369 doi: 10.1029/2011rg000369

Tomassini, L. (2020, August). The interaction between moist convection and the atmospheric circulation in the tropics. *Bulletin of the American Meteorological Society*, *101*(8), E1378–E1396. Retrieved from https://doi.org/10.1175/bams-d-19-0180.1 doi: 10.1175/bams-d-19-0180.1

Tsai, W.-M., & Wu, C.-M. (2017, September). The environment of aggregated deep convection. *Journal of Advances in Modeling Earth Systems*, *9*(5), 2061–2078. Retrieved from https://doi.org/10.1002/2017ms000967 doi: 10.1002/2017ms000967

Turbeville, S. M., Nugent, J. M., Ackerman, T. P., Bretherton, C. S., & Blossey, P. N. (2022, February). Tropical cirrus in global storm-resolving models: 2. cirrus life cycle and top-of-atmosphere radiative fluxes. *Earth and Space Science*, *9*(2). Retrieved from https://doi.org/10.1029/2021ea001978 doi: 10.1029/2021ea001978

van den Heever, S. C., & Cotton, W. R. (2007, June). Urban aerosol impacts on downwind convective storms. *Journal of Applied Meteorology and Climatology*, *46*(6), 828–850. Retrieved from https://doi.org/10.1175/jam2492.1 doi: 10.1175/jam2492.1

van den Heever, S. C., Stephens, G. L., & Wood, N. B. (2011, April). Aerosol indirect effects on tropical convection characteristics under conditions of radiative–convective equilibrium. *Journal of the Atmospheric Sciences*, *68*(4), 699–718. Retrieved from https://doi.org/10.1175/2010jas3603.1 doi: 10.1175/2010jas3603.1

Varble, A. (2018, April). Erroneous attribution of deep convective invigoration to aerosol concentration. *Journal of the Atmospheric Sciences*, *75*(4), 1351–1368. Retrieved from https://doi.org/10.1175/jas-d-17-0217.1 doi: 10.1175/jas-d-17-0217.1

Windmiller, J. M., & Hohenegger, C. (2019, December). Convection on the edge. *Journal of Advances in Modeling Earth Systems*, *11*(12), 3959–3972. Retrieved from https://doi.org/10.1029/2019ms001820 doi: 10.1029/2019ms001820

Wing, A. A., Emanuel, K., Holloway, C. E., & Muller, C. (2017, February). Convective self-aggregation in numerical simulations: A review. *Surveys in Geophysics*, *38*(6), 1173–1197. Retrieved from https://doi.org/10.1007/s10712-017-9408-4 doi: 10.1007/s10712-017-9408-4

Wing, A. A., & Emanuel, K. A. (2014, February). Physical mechanisms controlling self-aggregation of convection in idealized numerical modeling simulations. *Journal of Advances in Modeling Earth Systems*, *6*(1), 59–74. Retrieved from https://doi.org/10.1002/2013ms000269 doi: 10.1002/2013ms000269

Wing, A. A., Reed, K. A., Satoh, M., Stevens, B., Bony, S., & Ohno, T. (2018, March). Radiative–convective equilibrium model intercomparison project.

Geoscientific Model Development, *11*(2), 793–813. Retrieved from https://doi.org/10.5194/gmd-11-793-2018 doi: 10.5194/gmd-11-793-2018

Wing, A. A., Stauffer, C. L., Becker, T., Reed, K. A., Ahn, M.-S., Arnold, N. P., … Zhao, M. (2020, September). Clouds and convective self-aggregation in a multimodel ensemble of radiative-convective equilibrium simulations. *Journal of Advances in Modeling Earth Systems*, *12*(9). Retrieved from https://doi.org/10.1029/2020ms002138 doi: 10.1029/2020ms002138

Wu, C.-M., & Arakawa, A. (2014, May). A unified representation of deep moist convection in numerical modeling of the atmosphere. part II. *Journal of the Atmospheric Sciences*, *71*(6), 2089–2103. Retrieved from https://doi.org/10.1175/jas-d-13-0382.1 doi: 10.1175/jas-d-13-0382.1

Yanase, T., Nishizawa, S., Miura, H., & Tomita, H. (2022, September). Characteristic form and distance in high-level hierarchical structure of self-aggregated clouds in radiative-convective equilibrium. *Geophysical Research Letters*, *49*(18). Retrieved from https://doi.org/10.1029/2022gl100000 doi: 10.1029/2022gl100000

Yang, G.-Y., & Slingo, J. (2001, April). The diurnal cycle in the tropics. *Monthly Weather Review*, *129*(4), 784–801. Retrieved from https://doi.org/10.1175/1520-0493(2001)129<0784:tdcitt>2.0.co;2 doi: 10.1175/1520-0493(2001)129⟨0784:tdcitt⟩2.0.co;2

Zhang, C., & Ling, J. (2017, May). Barrier effect of the indo-pacific maritime continent on the MJO: Perspectives from tracking MJO precipitation. *Journal of Climate*, *30*(9), 3439–3459. Retrieved from https://doi.org/10.1175/jcli-d-16-0614.1 doi: 10.1175/jcli-d-16-0614.1

Supporting Information for "Modulation of Tropical Convection-circulation Interaction by Aerosol Indirect Effects in Idealized Simulations of a Global Convection-permitting Model"

Chun-Yian Su[1,2], Chien-Ming Wu[2], Wei-Ting Chen[2], and John M. Peters[1]

[1]Department of Meteorology and Atmospheric Science, The Pennsylvania State University, University Park, PA

[2]Department of Atmospheric Sciences, National Taiwan University, Taipei city, Taiwan

Contents of this file

1. Figures S1 to S3

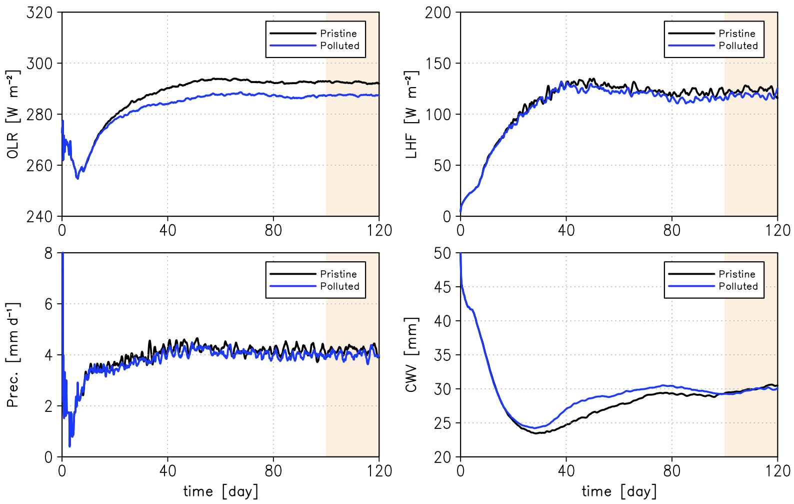

Figure S1. Time series of the global average of outward longwave radiation (upper left), surface latent heat flux (upper right), surface precipitation intensity (lower left), and column waver vapor (lower right). Day 100 to 120 is shaded.

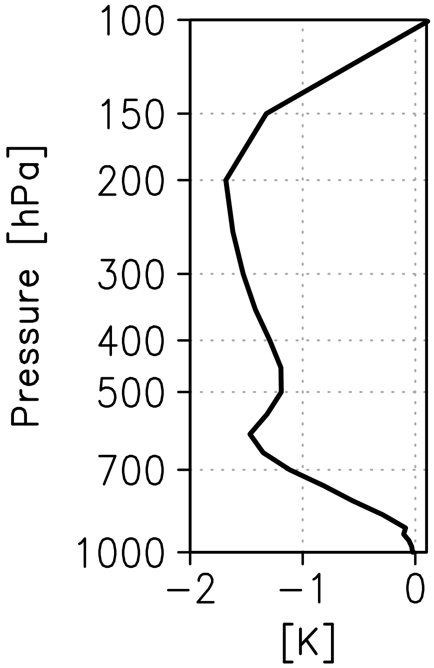

Figure S2. Difference in the global average of atmospheric temperature profile from day 100 to 120 between the polluted run and the pristine run.

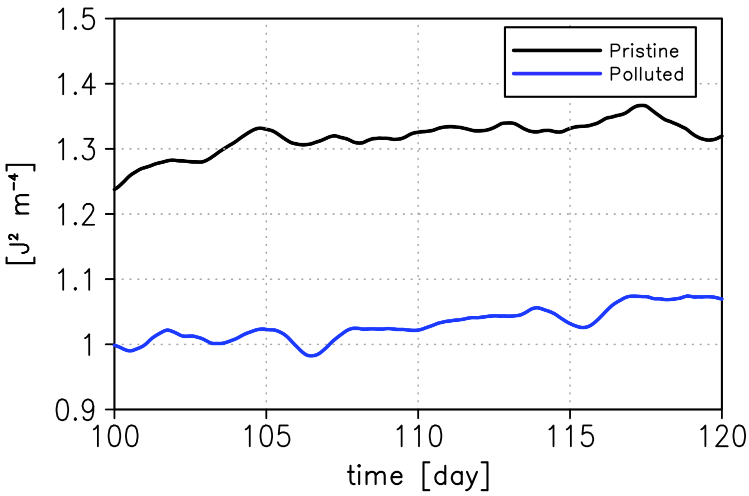

Figure S3. Time series of the spatial variance of vertically integrated FMSE.